Characterization of the nuclear import and export signals of the E7 protein of human papillomavirus type 11

Author: Courtney Holmes McKee

Boston College
Biology Department
Scholar of the College Thesis

Characterization of the nuclear import and export signals of the E7 protein of low risk human papillomavirus type 11

Courtney McKee
Advised by Dr. Junona Moroianu
April 2011

Table of Contents Page

Characterization of the nuclear import and export signals of the E7 protein of low risk human papillomavirus type 11

Courtney McKee
Advised by Dr. Junona Moroianu
April 2011

Abstract

The E7 protein of low risk human papillomavirus type 11 has been shown to interact with multiple proteins key to viral function, including pRb and other pocket proteins, in both the cytoplasm and the nucleus. It has been previously demonstrated that high risk HPV16 E7 and low risk HPV11 E7 share a novel nuclear import pathway independent of karyopherin proteins but dependent on the small GTPase Ran (Angeline, et al., 2003; Knapp, et al., 2009; Piccioli, et al., 2010). In this study, we continued the analysis of the nucleocytoplasmic transport of HPV11 E7 *in vivo* through transient transfection assays in HeLa cells with EGFP-HPV11 E7 fusion constructs and mutagenesis of critical amino acids.

We found that nuclear localization of HPV11 E7 is mediated by a nuclear localization signal located in the C-terminal domain (cNLS). This cNLS contains a unique zinc-binding domain consisting of two copies of a Cys-X-X-Cys sequence motif separated by 29 amino acids. To examine the role of the zinc-binding domain in HPV11 E7's nuclear localization mediated by the cNLS, we mutated cysteine residues in each of the two copies of the Cys-X-X-Cys motif. After transient transfection in HeLa cells, we analyzed the localization of the resultant EGFP-11cE7 mutants and EGFP-11E7 mutants in comparison with the corresponding wild type proteins using confocal fluorescence microscopy. We discovered that mutations of cysteine residues in the two Cys-X-X-Cys motifs which affect the zinc binding clearly disrupted the nuclear localization of the EGFP-11cE7 and EGFP-11E7 mutants. These data suggest that the integrity of the zinc-binding domain is essential for the nuclear localization of HPV11 cE7 and HPV11 E7 mediated by the cNLS. Analysis of the localization of an EGFP-11E7$_{32SS/AA}$ mutant, which cannot be phosphorylated by CKII, in comparison with the EGFP-11E7 wild type, revealed that CKII phosphorylation is not required for the nuclear localization of HPV11 E7. In

addition, we discovered that HPV11 E7 has a leucine-rich nuclear export signal (NES) located at the C-terminus ($_{76}$IRQLQDLLL$_{84}$) mediating the nuclear export of HPV11 E7 in a CRM1-dependent manner. We will continue our mutational-functional analysis to further examine the nucleocytoplasmic transport of the low risk human papillomavirus type 11 E7 oncoprotein.

Abbreviations:

HPV: human papillomavirus
pRB: retinoblastoma protein
NPC: nuclear pore complex
Kap: karyopherin
CKII: casein kinase II
NLS: nuclear localization signal
NES: nuclear export signal
EGFP: enhanced green fluorescent protein
HeLa: Henrietta Lacks, originator; HPV18+ cervical epithelial carcinoma cell line
RJA: ratjadone A, CRM-1 inhibitor
CRM-1: chromosome region maintenance 1 (exportin 1), export receptor
HA: hemagglutinin
FG: phenylalanine/glycine repeats

List of Figures Page

Acknowledgements

I would like to extend my thanks to Professor Junona Moroianu for her invaluable mentorship over the past four years. Professor, your guidance has been my anchor. It has been my great privilege to be your student and work under your tutelage.

To all members of the Moroianu Lab, thank you for creating a marvelous environment in which to work and to learn. I would particularly like to thank: Jeremy Eberhard, for many hours of training, troubleshooting, consultations, and brainstorming; Shahan Mamoor, for his instruction and advice; Zachary Piccioli, for assimilating me into his project and providing assistance as I began my work; and all other graduate students, undergraduate students, and technicians, for their enthusiasm and humor which buoy us all along. I have also been the beneficiary of the assistance of a number of Boston College biology department faculty and staff. I would like to mention in particular the generosity of Joshua Rosenberg, who invested his time and energy to train me in microscopy techniques. I am indebted to the Arnold and Mabel Beckman Foundation for their generous grant which supported my work.

To all of my family and friends, your continued and unflagging support means more than I can say. I am so blessed to have you in my life.

Introduction

I. Human papillomaviruses

Human papillomaviruses (HPVs) are small, icosahedral, non-enveloped DNA tumor viruses with circular, double-stranded genomes approximately 8 kb in size (Longworth and Laimins, 2004). Of the approximately 200 identified HPV types, over 30 are known to infect anogenital and oropharyngeal mucosal epithelial tissue (zur Hausen, 2000).

HPV types are divided into five genera according to their evolutionary relationships and are designated as alpha, beta, gamma, mu, and nu HPVs. Gamma, mu, and nu papillomaviruses comprise approximately 10% of HPVs and are only rarely associated with cancer. Instead, they are implicated in the development of benign cutaneous papillomas (Doorbar, 2006). The alpha and beta genera encompass 90% of HPV types. Beta HPVs, including types 5 and 8, have been linked to non-melanoma skin cancers, particularly squamous cell carcinomas, in immunocompromised patients and individuals with the genetic disorder epidermodysplasia verruciformis (Pfister, 2003). Alpha HPVs infect the anogenital mucosa as well as the skin and include cutaneous, high risk, and low risk types, classifications that correspond to their association with cancer development (Doorbar, 2006). Low-risk HPV types, the most common being 6 and 11, are associated with the formation of benign epithelial hyperplasias, including condyloma accuminata, or genital warts. Those classified as high risk, particularly types 16, 18, 31, and 45, show a marked propensity for malignant progression (Longworth and Laimins, 2004).

II. Human papillomaviruses and cancer

HPV is the most common sexually transmitted infection in the United States (Dunne, et al., 2007). As of 2004, 24.5% of females between 14 and 19 years old and 44.8% of females between 20 and 24 years old in the United States were infected with HPV (Dunne, et al., 2007). HPV DNA has been identified in over 99% of cervical cancers. Moreover, HPV16 and HPV18 infection account for nearly 70% of these cases (Dunne, et al., 2007). Cervical cancer is the second most common cancer in women worldwide after breast cancer, with 450,000 new cases diagnosed each year (Parkin, et al., 2002; Bodily and Laimins, 2010). A compelling link between HPV and cancer has been established not only in cervical cancers, but also in vulval, penile, oropharyngeal, tonsillar, and skin cancers (zur Hausen, 2009).

Approximately 90% of HPV infections clear without medical intervention within a few years (Dunne, et al., 2007). However, persistent infection occurs in roughly 10% of cases when the viral genome integrates into the host cell genome. The viral life cycle is intricately tied to the differentiation program in host cells (Moody and Laimins, 2010). The virus interacts with the basal lamina of the host, gaining access through microabrasions in the tissue. It then attaches to receptors on basal epithelium cells, thought to include integrin α6 and heparan sulfate proteoglycans, through interactions between the capsid protein L1 and these select moieties (Doorbar, 2006). After viral uptake into the cell, productive infection is dependent on host-cell machinery and is carefully regulated by viral proteins.

Oncogenic progression begins only upon the aberrant integration of the E6 and E7 oncogenes into the host genome, bypassing viral regulation by E2 and interfering with host cell-cycle controls (Doorbar, 2006). Though expression of E6 or E7 alone is not enough to fully transform normal epithelial cells, co-expression of E6 and E7 with the *ras* or *fos* oncogenes highly increases the risk of tumorigenesis (zur Hausen, 2000). These two major transforming proteins play a key role by interfering with numerous proteins involved in the cell-cycle regulation of host cells.

III. The E7 major transforming protein

The HPV E7 oncoprotein is an acidic, 98 amino acid long polypeptide. It has a 38 amino acid long amino terminus in an extended conformation that contains a Retinoblastoma protein (pRb) binding domain and a casein kinase II (CKII) consensus phosphorylation site (McLaughlin-Drubin and Munger, 2008; Knapp, et al., 2009). The highly ordered carboxyl terminus of E7, amino acids 39-98, includes a tightly folded zinc-binding domain, a nuclear localization signal (NLS), and a nuclear export signal (NES) (Angeline, et al., 2003, Knapp, et al., 2009; McLaughlin-Drubin and Munger, 2008). It has been proposed that the cysteine rich C-terminus is involved in E7 dimerization *in vivo*, though it has not been shown whether this dimerization is necessary for E7 function (Clemens, et al., 1995).

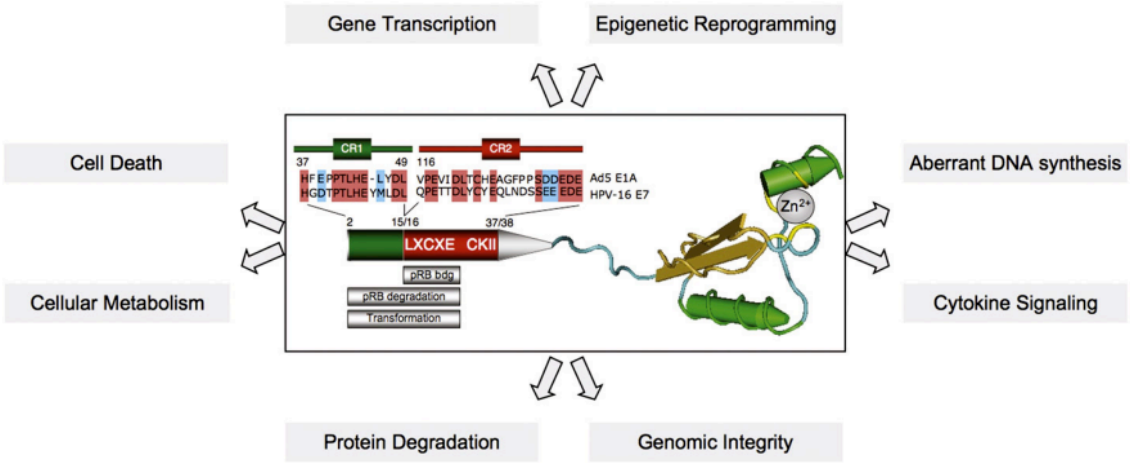

Figure 1. Schematic representation of the HPV E7 oncoprotein and affected cellular processes (McLaughlin-Drubin and Munger, 2008).

The E7 oncoprotein has multiple molecular targets in the cell in both the nucleus and the cytoplasm. E7 has been shown to bind and inactivate Retinoblastoma protein (pRb), a major modulator of cell-cycle progression, along with other pocket proteins such as p130 and p107 (McLaughlin-Drubin and Munger, 2008). Interestingly, high risk HPV16 E7 binds pRb ten times more efficiently than low risk HPV6 E7 due to a one amino acid change in the pRb binding site at residue 22, from aspartic acid in the high risk to glycine in the low risk (Heck, et al., 1992). E7 interferes with pRb activity within the cell by targeting the protein for proteosomal degradation, disrupting its regulation of E2F transcription factors and allowing the activation of proliferative pathways irrespective of host growth factors (McLaughlin-Drubin and Munger, 2008; Doorbar, 2006). As a result, cyclin production increases, driving the cell cycle forward. This outcome is compounded by E7's interference with the cyclin-dependent kinase inhibitors p21 and p27 which further contributes to a proliferative phenotype in infected cells (McLaughlin-Drubin and Munger, 2008). Interactions have also been recorded between E7 and p600, a novel microtubule-associated protein. The proposed downregulation of p600 by E7 is thought to correlate with the prevention of anoikis in infected cells, allowing the perpetuation of a transformed phenotype (McLaughlin-Drubin and Munger, 2008). The multiple interactions of E7 and proteins in both the nucleus and the cytoplasm indicate the importance of its function to viral activity in both compartments. It is therefore critical that the pathways that mediate its trafficking are elucidated.

IV. Nuclear Import and Export

The nuclear pore complex (NPC) forms a semi-permeable, selective barrier between the cytoplasmic and nuclear compartments. It is an approximately 50 MDa complex, 100 nm in diameter, comprised of rings of nucleoporin proteins spanning the nuclear membrane (Alber, et al., 2007). Approximately 30 different kinds of nucleoporins are oriented according to an eight-fold, radially symmetric arrangement (Sorokin, et al., 2007). Additional nucleoporins extend into both the nuclear and cytoplasmic compartments. Within the nucleus, these nucleoporins are arranged into a basket-like structure; in the cytoplasm, they form linear spokes that extend outward. These extended nucleoporins form a channel that allows for the passive diffusion of smaller molecules and proteins and also provide sites of interaction for larger cargoes which may then be translocated through the NPC (Sorokin, et al,. 2007; Alber, et al., 2007). The ability to passively diffuse is limited to cellular components of less than 40 kD, but when facilitated by cellular import and export factors, cargoes on the order of a few megadaltons can be trafficked efficiently through the NPC (Ribbeck and Gorlich, 2002).

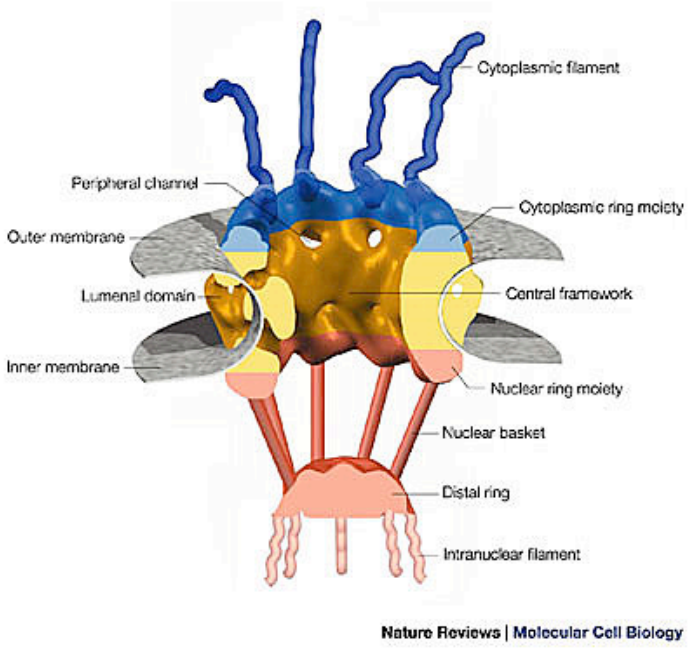

Figure 2. Schematic representation of the NPC (Fahrenkrog, B. and Aebi, U., 2003).

Facilitated import and export of cargoes between the nucleus and cytoplasm is mediated by a variety of receptor proteins and adapters. A family of proteins called karyopherins (Kaps) can bind nuclear localization signals (NLSs) and nuclear export signals (NESs) on a cargo protein directly or interact with cargo through an adapter Kap (Moroianu, 1999). Characteristic of Kaps is the additional ability to interact with the small GTPase Ran in its GTP bound state (Moroianu, 1999). The canonical import pathway involves the binding of a Kap, referred to as an importin, to a protein's NLS. The resultant complex is translocated though the NPC via interactions with nucleoporins and dissociates within the nucleus upon binding of the small

GTPase Ran in its GTP bound form (Moroianu, 1999). Nuclear export occurs upon the binding of a Kap, known as an exportin, to the nuclear export signal (NES) of a protein as well as Ran-GTPase in its GTP bound form within the nucleus (Pemberton and Paschal, 2005). This receptor-cargo-Ran-GTP tertiary complex is then translocated through the NPC and dissociates in the cytoplasm upon the hydrolysis of Ran-GTP to Ran-GDP (Pemberton and Paschal, 2005). The accessory components of these pathways, including the import and export receptors, are then recycled to their original compartments.

V. Nucleocytoplasmic transport of high risk HPV16 E7 and low risk HPV11 E7

It has been recently established that high risk HPV16 E7 enters the nucleus through a novel, Ran-dependent pathway, independent of Kap β1, Kap β2, or Kap α2/β1 heterodimers (Angeline, et al., 2003; Knapp et al., 2009). This import is mediated via a C-terminal NLS as well as a hypothesized N-terminal NLS (Knapp, et al., 2009). Interestingly, the C-terminal domain of HPV16 E7 contains both an NES and an NLS and ultimately presents a mostly cytoplasmic phenotype (Knapp, et al., 2009). The C-terminal domain of HPV11 E7, however, displays a mostly nuclear phenotype (Piccioli, et al., 2010). To begin the characterization of the nuclear import of HPV11 E7, it was noted that the highly ordered C-terminal domain of HPV11 E7 includes a unique zinc-binding domain that encompasses both a previously observed NLS as well as a putative NES that shares distinct sequence homology with the NES of HPV16 E7 (Knapp, et al., 2009). The goals of this study include the characterization of the role of the zinc-binding domain of HPV11 E7 in the protein's nuclear import and export as well as the characterization of the putative leucine-rich NES of HPV11 E7.

Materials and Methods

Cell Culture

ATCC (American Type Culture Collection) HeLa cells, an HPV18+ cervical epithelial carcinoma cell line, were cultured in Dulbeccos Modified Eagle Medium (DMEM) with 10% heat-inactivated fetal bovine serum (FBS) and 1% penicillin-streptomycin solution (5,000 units penicillin and 5 mg streptomycin per mL). The cells were maintained at 37°C in 5% CO_2.

Antibodies

A GFP-α-mouse antibody (Clontech, Inc.) and a HRP-conjugated goat-α-mouse antibody (Santa Cruz Biotechnology, Inc) were used.

Generation of EGFP fusion plasmids with HPV11 E7 wild type, HPV11 E7 N- and C-terminal domains, and HPV11 E7 and HPV11 cE7 mutants

EGFP-tagged HPV11 E7 fusion constructs, including the full length protein and fragments with amino acids 1-38 and 39-98, were established in the expression plasmid pEGFP-C1 (Clontech, Inc). These constructs were generated by other members of the Moroianu Lab as follows: the pEGFP-C1 plasmid was double digested with EcoR1 and BamH1, run on a 0.7% agarose gel, and the digested vector was extracted using a QIAquick Gel Extraction Kit (Qiagen). DNA fragments spanning the full length HPV11 E7 or the C-terminal domain (aa 39–98) were amplified using PCR oligonucleotides that added EcoR1 and BamH1 restriction endonuclease sites. The PCR products were digested with EcoR1 and BamH1 restriction enzymes and then ligated using T4 DNA ligase into the EcoR1 and BamH1 cloning sites of pEGFP-C1. The EGFP-11E7$_{1–38}$ was generated using the QuikChange™ Site-Directed Mutagenesis Kit (Stratagene) with EGFP-11E7 as a template together with mutated primers to delete amino acids 39-98. The EGFP tag is located at the N-terminus of all constructs (Piccioli, et al., 2010).

Oligonucleotide primers were designed and optimized for each mutant (Sigma-Genosys). All primers were HPLC purified. The EGFP-11cE7$_{C58A}$, EGFP-11cE7$_{57CCC/AAA}$, EGFP-11cE7$_{C91A}$, EGFP-11cE7$_{C91_}$ mutant plasmids were generated using the QuikChange™ Site-Directed Mutagenesis Kit (Stratagene) with EGFP-11cE7 as a template together with the corresponding mutated primers. The same mutations, with the exception of the C91_ mutant, were also introduced in the context of EGFP-11E7 using the corresponding mutated primers. Lastly, additional mutants, EGFP-11E7$_{C58A/L79A}$ and EGFP-11E7$_{C58A/82LLL/AAA}$, EGFP-11E7$_{C91A/L79A}$, and EGFP-11E7$_{C91A/82LLL/AAA}$, were generated in the context of either the EGFP-11E7$_{C58A}$ or EGFP-11E7$_{C91A}$ mutant plasmid using the corresponding mutant primers. The EGFP-11cE7$_{C59A}$, EGFP-11cE7$_{C59D}$, EGFP-11E7$_{C59A}$, and EGFP-11E7$_{C59D}$ mutants were generated by Zeynep Onder, a member of the Moroianu Lab.

The mutant fusion plasmids were transformed into XL1-blue competent cells. Cultures were plated onto 45 ng/μL kanamycin-LB agar plates. Colonies were transferred to 10 mL LB cultures with 1:1000 kanamycin and grown overnight at 37°C and 235 rpm. Plasmids were extracted using a Quantum Prep® Plasmid MiniPrep kit (BioRad). The purified mutant DNA was analyzed for size by agarose gel electrophoresis and the sequence was obtained by direct sequencing (Eurofins MWG). Verified mutant plasmids were maintained as stock cultures with glycerol at -80°C.

Purification of recombinant EGFP-E7 fusion plasmids

Plasmids stored in XL1 Blue *E. coli* cells, maintained as stock cultures at -80°C, were grown in 50mL of LB with 1:1000 kanamycin overnight at 37°C and 235 rpm. The plasmids were then purified using a Quantum Prep® Plasmid MidiPrep kit (BioRad). The plasmids were analyzed for appropriate molecular weight and purity using agarose gel electrophoresis. The concentration of each plasmid was obtained using a NanoDrop™ 2000 spectrophotometer (Thermo Scientific).

Transfection assays and confocal fluorescence microscopy analysis

HeLa cells were grown on 12 mm poly-L-lysine-coated glass cover slips for 24 h prior to transfection until 50-70% confluent. A mixture of 3μL FuGENE 6 reagent (Roche Applied Science) and 0.6 μg of plasmid DNA was added to 97μL DMEM and incubated at RT for 20 min to allow complex formation. The cells were placed in 500μL DMEM and the DNA/FuGENE solution was added to the cells. After 5 h, the media was switched to 500μL DMEM with 1% penicillin-streptomycin and 10% FBS (DMEM+). After 24 h, the cells were washed with 1xPBS (pH 7.4) three times for 3 min each. The cells were fixed in 3.7% formaldehyde in 1xPBS for 10 min and washed an additional three times with 500μL 1xPBS for 3 min each. The cover slips were mounted on glass slides using VectaSheild-DAPI Mounting Media with DAPI (Vector Labs) for the visualization of the cell nuclei. The cover slips were sealed to the slides with clear nail polish. The slides were kept covered at 4°C until analysis. Detection of EGFP-fusion proteins was performed using a Leica TCS Sp5 broadband confocal microscope (Leica Microsystems), and pictures were taken using Leica LAS AF software (Leica Microsystems). Quantification of the intracellular phenotypes, defined as mostly nuclear, pancellular, or mostly cytoplasmic, was performed on all transfections. Data from at least four experiments was

compiled for the quantitative analysis and the graphical representations display averages with standard deviation.

Ratjadone A treatment of transfected cells

A 10 ng/mL solution of Ratjadone A (RJA) in DMEM+ was added to transfected cells at 20 h post transfection for 4 h. A parallel transfection received no RJA treatment, but instead received fresh DMEM+ at 20 h post transfection.

Immunoblot assays of transfected cells

Transfected cells were transferred to SDS-PAGE buffer with 1% β-mercapatoethanol, lysed, boiled for 10 min at 100°C, and vortexed. The samples were then subjected to SDS-polyacrylamide gel electrophoresis. Transfer to a nitrocellulose membrane was performed at 60V in Tris-Glycine buffer for 60 min. Ponceau staining was used to visualize the proteins on the membrane and confirm equivalent protein loading. Samples were blocked in 5% nonfat milk in 1xPBS (pH 7.4) for 1 h at RT or overnight at 4°C. They were then incubated at RT for 1 h in a 1:2000 GFP-α-goat antibody solution. Samples underwent three 5 min washes in 1xPBS, and were then incubated for 30 min in a 1:1500 HRP-conjugated goat-α-mouse antibody solution. Detection was performed using an ECL Detection Kit (GE Healthcare) and exposure with X-ray film (Denville Scientific Inc.) was done using an XO-MAT developer (Kodak).

Results

Immunoblot analysis of HPV11 cE7, HPV11 E7, and mutant proteins

In order to ensure that the proteins expressed in HeLa cells during transfection assays were the appropriate molecular weight and not degraded *in vivo*, EGFP tagged HPV11 E7 wild types and mutant proteins were compared to an EGFP standard in an immunoblot analysis (Figures 4A and 4B). After detection with an anti-GFP antibody, the EGFP standard (Figures 4A and 4B, Lane 1), a 28kD protein, was compared to that of the HPV11 E7 wild type and mutant proteins. All of the recombinant proteins ran at a higher molecular weight and did not show degradation. This confirmed that the proteins detected during fluorescence microscopy were intact proteins.

Localization of wild type EGFP-11E7, EGFP-11cE7, and EGFP-11nE7 *in vivo*

The equilibrium localization of wild type HPV11 E7, the N-terminal region of HPV11 E7 (aa 1-38), and the C-terminal region of HPV11 E7 (aa 39-98) were analyzed in transfection assays. The full-length EGFP-11E7 and the C-terminal domain of EGFP-11E7 presented a mostly nuclear phenotype in HeLa cells (Figure 5A). Approximately 80% of cells transfected with either EGFP-11E7 or EGFP-11cE7 showed the proteins localized to the nucleus, while the remaining cells had a pancellular localization (Figure 5B). The N-terminal domain of EGFP-11E7 was shown to have a pancellular phenotype in 70% of cells and a mostly cytoplasmic phenotype in approximately 30% of cells (Figure 5A; Figure 5B). The similar localization to the nucleus of both the C-terminal region and the full-length HPV11 E7 suggests that the nuclear import of HPV11 E7 is mediated by a nuclear localization signal in the C-terminal domain (cNLS).

Nuclear import of HPV11 E7 is not dependent on CKII phosphorylation

To investigate whether CKII phosphorylation is a factor in the nuclear localization of HPV11 E7, two serines at positions 32 and 33 known to participate in CKII phosphorylation were mutated to alanine, a non-polar amino acid that cannot participate in CKII phosphorylation (McLaughlin-Drubin and Munger, 2008). There was no observed change in localization in the EGFP-11E7$_{32SS/AA}$ phosphorylation deficient mutant as compared to the wild type EGFP-11E7 protein (Figure 6): both localized to the nucleus in approximately 80% of transfected cells (Figure 5B). Because the $_{32}$SS/AA mutation did not affect the nuclear localization of HPV11 E7, we conclude that the nuclear import of HPV11 E7 is not dependent on CKII phosphorylation.

The integrity of the C-terminal zinc-binding domain of HPV11 E7 is necessary for its nuclear localization *in vivo*

HPV11 E7's zinc binding domain provides a highly ordered structure for the protein's C-terminal region. Four cysteine residues at positions 58, 61, 91, and 94 conjugate a Zn^{2+} ion between them in a planar conformation, and the intervening sequence is arranged in a helix-loop-alpha conformation (McLaughlin-Drubin and Munger, 2008). To determine whether the zinc-binding ability of HPV11 E7 is necessary for its nuclear localization, we mutated different

cysteine residues involved in zinc-binding to alanine in the context of both HPV11 E7 and HPV11 cE7 (Figure 3A).

Mutations in the second Cys-X-X-Cys sequence motif of HPV11 cE7, specifically the cysteine residue at position 91 to alanine or a deletion of the final 8 amino acids of HPV11 E7, resulted in a marked change in its localization. As compared to the mostly nuclear wild type, the C91A and C91_ HPV11 cE7 mutants were observed to be mostly cytoplasmic in over 90% of transfected cells (Figure 8B, panels B and C; Figure 8C). The C91A mutation in the context of the HPV11 E7 full length protein also resulted in a similar change in the localization, becoming mostly cytoplasmic in greater than 90% of cells (Figure 7A, panel E; Figure 7B). These results indicated that zinc-binding deficient mutants were unable to localize to the nucleus.

To further analyze the zinc-binding domain, mutations in the first Cys-X-X-Cys sequence motif were performed. Initial mutants converting the cysteine at position 58 to alanine in both the HPV11 E7 and HPV11 cE7 also displayed diminished nuclear localization. The majority of cells transfected with either EGFP-11E7$_{C58A}$ or EGFP-11cE7$_{C58A}$ displayed a pancellular phenotype in over 70% of cells (Figure 7B; Figure 8A, panel C; Figure 8C, data not shown). The remaining 30% of cells displayed a mostly cytoplasmic localization of the mutant protein (Figure 7B; Figure 8C). This intermediate phenotype, less dramatic than that seen in the C91_ or C91A mutants, suggested to us that neighboring cysteines at positions 57 and 59 may have countered the loss of zinc-binding ability in the C58A mutant. These neighboring cysteines may have then restored partial function to the cNLS, allowing localization of some EGFP-11E7$_{C58A}$ and EGFP-11cE7$_{C58A}$ to the nucleus.

A final mutant with all three cysteines at positions 57, 58, and 59 converted to alanine was generated to confirm this hypothesis (Figure 3A). In both the context of the HPV11 cE7 and the HPV11 E7, the localization of this mutant was mostly cytoplasmic in over 90% of cells (Figure 8A, Panel E; Figure 7A, Panel C; Figure 8C; Figure 7B). This dramatic phenotype was very similar to that seen in the C91A and C91_ mutants. Whereas in the C58A mutant, adjacent cysteines could restore zinc binding, allowing the mutant to localize to the nucleus to a lesser degree, the triple cysteine to alanine mutant was not able to localize to the nucleus. Given the decrease observed in the nuclear localization of all of the zinc-binding deficient mutants, the zinc-binding ability of HPV11 E7 is necessary for the nuclear localization of the protein. These

data confirmed that the structural integrity of the zinc-binding domain of HPV11 E7 is required for the activity of its cNLS.

A conserved cysteine residue at position 59 is involved in HPV11 E7's nuclear localization

Structural studies suggest that the conserved cysteine at position 59 is not directly involved in zinc-binding (Ohlenschlager, et al., 2006). To investigate the role of the cysteine at position 59 in the nuclear localization of HPV11 E7, a mutation of this cysteine to alanine was performed in the context of the HPV11 cE7 and HPV11 E7. This alteration resulted in a mostly pancellular distribution of the mutant protein (Figure 9A, Panels C and G) in comparison to the mostly nuclear wild type (Figure 9A, Panels A and E). Approximately 80% of cells had a pancellular phenotype, while the remaining 20% displayed a mostly nuclear phenotype (Figure 9B).

It is thought that the cNLS of HPV11 E7 may interact with the nuclear pore complex through low-affinity hydrophobic interactions with phenylalanine-glycine (FG) repeats in nucleoporins in order to translocate into the nucleus, as previously shown for nuclear import receptors (Piccioli, et al., 2010; Ribbeck and Gorlich, 2002). The conversion of a cysteine residue to a polar, acidic residue, aspartic acid, would diminish these hydrophobic interactions. We generated C59D mutants in both the context of HPV11 cE7 and HPV11 E7, and in both cases, the phenotype observed was pancellular in over 90% of cells (Figure 9B). These data indicated that the cysteine at position 59 is involved in the nuclear localization of HPV11 E7, as its removal reduced the nuclear localization of the mutant.

The RJA nuclear export inhibitor partially restores the nuclear localization of the HPV11 E7 and HPV11 cE7 C58A and C91A mutants

The major nuclear export receptor CRM1 has been shown to interact with leucine-rich NESs like those found in HPV16 E7 (Fornerod, et al., 1997; Knapp, et al., 2009). To begin our analysis of the putative leucine-rich NES of HPV11 E7, we treated transfected cells with the CRM1 inhibitor RJA and analyzed the localization of cells given the drug in comparison to an untreated control. The positive control, designated HPV16E7-NES, is a fusion of HPV16 E7 and the NES of HIV-1 Rev, a leucine-rich NES known to interact with CRM1 (Malim, et al., 1991; Fornerod, et al., 1997). Wild type HPV16 E7 has a predominantly nuclear phenotype (Knapp, et al., 2009). However, upon the addition of the HIV-1 Rev NES to the C-terminus of HPV16 E7,

the protein localizes to the cytoplasm in approximately 90% of transfected cells (this report, Figure 10B). Treatment with RJA prompts in a change in the localization back to nuclear in over 90% of transfected cells (this report, Figure 10B).

When cells transfected with EGFP-11E7 were treated with RJA, approximately 90% of the cells had a mostly nuclear phenotype (Figure 10A, Panels C and D; Figure 10B). This was a slight increase from the untreated wild type, for which 80% of the cells had a mostly nuclear phenotype (Figure 10A, Panels A and B; Figure 10B). Additionally, this pattern was also seen in transfections performed with the EGFP-11cE7. Whereas the EGFP-11cE7 protein localizes to the nucleus in 80% of cells, treatment with RJA resulted in 90% of cells having a mostly nuclear phenotype (Figure 11A, Panels A-D; Figure 11B). These data suggested that HPV11 E7 has a functional NES located in its C-terminal domain whose activity can be diminished through RJA's inhibition of CRM1.

To further examine the nuclear export activity of HPV11 E7, we examined effect of RJA treatment on the behavior of two zinc-binding deficient mutants, C58A and C91A, in the context of both the HPV11 E7 and HPV11 cE7. After treatment with RJA, cells transfected with the EGFP-11E7$_{C91A}$ mutant had a mostly nuclear phenotype in approximately 55% of cells, while the remaining cells had a pancellular phenotype (Figure 10A, Panels K and L; Figure 10B). This was a dramatic change from the untreated EGFP-11E7$_{C91A}$, which had a mostly cytoplasmic localization in 90% of transfected cells (Figure 10A, Panels I and J; Figure 10B). Similarly, after treatment with RJA, the EGFP-11E7$_{C58A}$ also had a mostly nuclear phenotype in approximately 55% of cells, while the remaining cells had a pancellular phenotype (Figure 10A, Panels G and H; Figure 10B). This was a significant change from the untreated EGFP-11E7$_{C58A}$, which was observed to have a mostly cytoplasmic phenotype in approximately 35% of cells, and a pancellular phenotype in the remaining cells (Figure 10A, Panels E and F; Figure 10B). Overall, treatment with RJA partially restored the nuclear localization of both the EGFP-11E7$_{C91A}$ and the EGFP-11E7$_{C58A}$ zinc-binding deficient mutants.

EGFP-11cE7$_{C58A}$ and EGFP-11cE7$_{C91A}$ transfected cells, when treated with RJA, also showed a partial recovery of their nuclear localization, though to a lesser extent. Cells transfected with the EGFP-11cE7$_{C91A}$ mutant in the presence of RJA had a mostly nuclear phenotype in approximately 10% of cells, a pancellular phenotype in approximately 75% of cells, while the remaining cells had a mostly cytoplasmic phenotype (Figure 11A, Panels K and

L; Figure 11B). This represented a change from the phenotype of the untreated EGFP-11cE7$_{C91A}$, which was mostly cytoplasmic in over 90% of transfected cells (Figure 11A, Panels I and J; Figure 11B). Treatment of the EGFP-11cE7$_{C58A}$ transfected cells with RJA also resulted in a change in the localization of the protein. Treated cells had a mostly nuclear phenotype in approximately 15% of cells, a pancellular phenotype in approximately 80% of cells, while the remaining cells had a mostly cytoplasmic phenotype (Figure 11A, Panels G and H; Figure 11B). Untreated cells transfected with the EGFP-11cE7$_{C58A}$ had a pancellular localization in approximately 65% of cells and a mostly cytoplasmic localization in the remaining cells (Figure 11A, Panels E and F; Figure 11B). Though the effect of RJA on the behavior of the zinc-binding mutants C58A and C91A in the context of the HPV11 cE7 was less dramatic than the change observed in the HPV11 E7 mutants, there was nevertheless a partial restoration of the nuclear localization of both the EGFP-11cE7$_{C91A}$ and the EGFP-11cE7$_{C58A}$ after treatment with RJA. These data suggest that HPV11 E7 has a functional NES located in its C-terminal domain that interacts with CRM1 and whose activity can be partially inhibited by the CRM1 inhibitor RJA.

Mutations of critical leucine residues in a potential cNES change the localization of the HPV11 E7 C58A and C91A mutants

Previous work in the Moroianu Lab has revealed that the C-terminus of HPV16 E7 contains a leucine-rich NES (Knapp, et al., 2009). This sequence, $_{76}$IRTLEDLLM$_{84}$, is highly conserved in HPV11 E7, particularly in the hydrophobic leucine (I/V/F/M) residues. In order to investigate the homologous sequence in HPV11 E7, $_{76}$IRQLQDLLL$_{84}$, we mutated critical leucine residues, one at position 79 and three at positions 82-84, in the context of both the EGFP-11E7$_{C91A}$ and EGFP-11E7$_{C58A}$ mutants (Figure 3B). In order to ensure that the proteins expressed in HeLa cells during transfection assays were the appropriate molecular weight and not degraded *in vivo*, EGFP tagged HPV11 E7 wild type and mutant proteins were compared to an EGFP standard in an immunoblot analysis (Figure 12). After detection with an anti-GFP antibody, the EGFP standard (Figure 12, Lane 1), a 28kD protein, was compared to that of the wild type HPV11 E7 and mutant proteins. All of the recombinant proteins ran at a higher molecular weight and did not show degradation. This confirmed that the proteins detected during fluorescence microscopy were intact proteins.

Both the EGFP-11E7$_{C91A/L79A}$ and EGFP-11E7$_{C91A/82LLL/AAA}$ mutants displayed altered phenotypes in comparison to the EGFP-11E7$_{C91A}$. The EGFP-11E7$_{C91A/L79A}$ displayed a mostly nuclear phenotype in approximately 20% of cells, a pancellular phenotype in approximately 75% of cells, and a mostly cytoplasmic phenotype in the remaining cells (Figure 13A, Panels E and F; Figure 13B). Similarly, the EGFP-11E7$_{C91A/82LLL/AAA}$ mutant also displayed a mostly nuclear phenotype in approximately 20% of cells, a pancellular phenotype in approximately 75% of cells, and a mostly cytoplasmic phenotype in the remaining cells (Figure 13A, Panels G and H; Figure 13B). This was a distinct change from the phenotype of the EGFP-11E7$_{C91A}$ mutant, which had a mostly cytoplasmic phenotype in 90% of transfected cells (Figure 13A, Panels C and D; Figure 13B).

The EGFP-11E7$_{C58A/L79A}$ and EGFP-11E7$_{C58A/82LLL/AAA}$ mutants also displayed an altered phenotype in comparison to the EGFP-11E7$_{C58A}$ mutant. The EGFP-11E7$_{C58A}$ mutant was mostly cytoplasmic in approximately 30% of cells and pancellular in the remaining 70% of cells. However, the EGFP-11E7$_{C58A/L79A}$ mutant localized to the nucleus in approximately 20% of cells, was pancellular in 75% of cells, and localized to the cytoplasm in the remaining 5% of cells (Figure 14A, Panels E and F; Figure 14B). The EGFP-11E7$_{C58A/82LLL/AAA}$ mutant had a slightly different distribution, with approximately 10% of cells displaying a mostly nuclear phenotype, 85% of cells a pancellular phenotype, and the remaining cells a mostly cytoplasmic phenotype (Figure 14A, Panels G and H; Figure 14B).

Overall, these data indicate that mutations in the critical leucine residues partially restored the nuclear localization of the HPV11 E7 C58A and C91A mutants. This suggests that the sequence $_{76}$IRQLQDLLL$_{84}$ is, indeed, the NES of HPV11 E7 and can mediate its nuclear export.

Discussion

HPV11 E7 has been shown to interact with multiple proteins key to viral function in both the cytoplasm and the nucleus, and its activity in both cellular compartments suggests an active trafficking pathway at work in infected cells. It has been previously demonstrated that HPV16 E7 and HPV11 E7 share a novel import pathway independent of Karyopherin proteins but dependent on the small GTPase Ran (Angeline, et al., 2003; Knapp, et al., 2009; Piccioli, et al.,

2010). Previous work in the Moroianu lab has suggested a possible nuclear import pathway for HPV11 E7 involving direct, low-affinity hydrophobic interactions with FG repeats in nucleoporins in a manner analogous to Kap import receptors (Piccioli, et al., 2010). In this study, we continued the analysis of the nucleocytoplasmic transport of HPV11 E7 *in vivo* through the investigation of the role of HPV11 E7's zinc-binding domain in its nuclear localization. Additionally, we examined the role of a putative leucine-rich cNES in HPV11 E7's nuclear export.

EGFP-tagged HPV11 E7 wild type and mutant proteins were used in transient transfection assays in HeLa cells. An N-terminal EGFP tag was used for the fusion proteins instead of a smaller tag, like an HA tag, to ensure that the fusion proteins were of a sufficient molecular weight to prevent passive diffusion into or out of the nucleus. Though both HPV11 E7 and HPV11 cE7 are under the passive diffusion limit of the NPC, HPV11 E7 is known to dimerize *in vivo* through a region in its C-terminal domain (Clemens et al., 1995). The resulting dimers, with their additional EGFP tags, are unable to undergo passive diffusion. The nuclear phenotypes of the EGFP-HPV11 E7 proteins were clearly distinct from the uniformly pancellular phenotype of a 1xEGFP control that can passively diffuse into and out of the nucleus. Additionally, the use of an EGFP tag allowed the elimination of an additional immunostaining step.

The EGFP-tagged wild type HPV11 E7 full length and HPV11 cE7 fusion proteins were observed to localize strongly to the nucleus, suggesting the presence of a C-terminal NLS. However, HPV11 E7, like HPV16 E7, lacks a classical monopartite or bipartite basic NLS (Angeline, et al., 2003). A CKII-phosphorylation deficient mutant HPV11 E7 was demonstrated to also have a mostly nuclear phenotype like the wild type, indicating that the nuclear import of HPV11 E7 is not dependent on CKII phosphorylation. To examine the hypothesized C-terminal NLS of HPV11 E7, we focused on the zinc-binding domain of HPV11 E7, a highly conserved region located in the C-terminus of the protein. Cysteine residues at position 58, 61, 91, and 94 complex a Zn^{2+} ion between them, resulting in a highly ordered, tightly folded C-terminal region (McLaughlin-Drubin and Munger, 2008). Mutant proteins with key cysteines converted to non-polar alanine residues would be deficient in stabilizing the Zn^{2+} ion, which could disrupt the structural integrity of the region.

These cysteine to alanine mutations, performed in the context of both HPV11 E7 full length and HPV11 cE7, were found to have a marked influence on the protein's localization phenotype. We observed dramatically decreased nuclear localization of the mutants in comparison to the wild type protein. The complete or partial loss of nuclear localization upon the disruption of the zinc-binding domain of HPV11 E7 indicates that this domain functions as the NLS of HPV11 E7. The tertiary structure of HPV11 E7's C-terminal domain established upon zinc-binding likely presents key amino acids that interact with FG-nucleoporins and allow the import of HPV11 E7. These data indicating that the zinc-binding domain of HPV11 E7 functions as the NLS mediating its nuclear import and localization have been recently published (Piccioli, et al., 2010). Interestingly, preliminary studies with the high risk HPV16 E7 also suggest that the zinc binding domain of HPV16 E7 is essential for its nuclear localization (Junona Moroianu and Jeremy Eberhard).

Additional analysis of the zinc-binding domain of HPV11 E7 examined the role of a conserved cysteine residue at position 59. This cysteine is not directly involved in zinc-binding, though its proximity to the involved cysteine residue at position 58 may provide additional stabilization of the zinc ion in the C58A mutant. Mutations to alanine and to aspartic acid in the context of both the HPV11 E7 full length and C-terminal domain both resulted in a diminished nuclear localization of the mutant proteins. Interestingly, while a diminished nuclear localization was observed in the C59A and C59D mutants, we did not observe cells with a mostly cytoplasmic phenotype, which would have indicated a complete loss of nuclear localization. This continued nuclear localization of the mutant proteins was subtle; for the EGFP-11cE7$_{C59A}$ mutant as well as the EGFP-11E7$_{C59D}$ and EGFP-11cE7$_{C59D}$ mutants, only approximately 5% of cells displayed a mostly nuclear phenotype. A slightly more marked nuclear phenotype was observed, however, in the EGFP-11E7$_{C59A}$ mutant, with approximately 20% of cells displaying a mostly nuclear phenotype (see Figure 9B). These data are in contrast to the pattern observed in experiments with the zinc-binding deficient mutants, which displayed pancellular and mostly cytoplasmic phenotypes. The partial maintenance of nuclear localization of the C59A and C59D mutants suggests some nuclear localization continues without cysteine 59. Further analysis is needed to elucidate the role of cysteine 59 in the nuclear import of HPV11 E7.

In our examination of the nuclear export pathway of HPV11 E7 with the nuclear export inhibitor RJA, we observed an increase in the nuclear phenotype in cells for both the full length

and C-terminal wild type HPV11 E7. Additionally, when cells transfected with the C58A and C91A zinc-binding deficient mutants in the context of both the full length HPV11 E7 and HPV11 cE7 were treated with RJA, we observed a partial recovery of nuclear localization of these mutants. These data indicate that HPV11 E7 contains an active NES in the C-terminus of HPV11 E7 that interacts with CRM1 to mediate export to the cytoplasm. Furthermore, the activity of HPV11 E7's cNES can be partially inhibited by the CRM1 inhibitor RJA.

We hypothesized that a leucine-rich sequence found at the C-terminus of HPV11 E7 was the cNES of HPV11 E7. This sequence, $_{76}$IRQLQDLLL$_{84}$, shares a high degree of homology with a sequence of HPV16 E7, $_{76}$IRTLEDLLM$_{84}$, which has been shown previously to be the cNES of HPV16 E7 (Knapp, et al., 2009). Mutations of critical leucine residues at position 79 or 82-84 converted to alanine disrupted the export activity of this region, but it is important to note that these mutations were introduced in the context of the zinc-binding deficient mutants C58A and C91A. Mutations of solely these leucine residues in the wild type HPV11 E7 or HPV11 cE7 would have been insufficient to indicate their involvement in the NES of HPV11 E7. The wild type proteins already demonstrate a distinctly nuclear phenotype, and inhibition of the NES in the wild type background would have been difficult to quantify. However, the C58A and C91A mutants had a consistent pancellular or mostly cytoplasmic phenotype, respectively. A change in the phenotype back to mostly nuclear upon a secondary NES mutation could then be observed and measured. We did observe a change in the phenotype of the C58A and C91A mutants in both the HPV11 E7 and HPV11 cE7 upon mutation of the leucine residues. There was a clear increase in the nuclear localization of these leucine mutants performed in the context of the C58A and C91A mutants. However, we did not observe a complete restoration to the mostly nuclear phenotype of the wild type protein. It is possible that with the added zinc-binding mutation, the doubly mutated proteins may have had some problems with folding and thus diminished import into the nucleus, lessening the effect of the export-blocking mutations. However, given the mitigating effect on nuclear export by the leucine mutations as well as by RJA, we suggest that the sequence $_{76}$IRQLQDLLL$_{84}$ is the NES of HPV11 E7.

Further work concerning the balance between the nuclear import and export of HPV11 E7, and the ramifications of this equilibrium, will be extremely intriguing. Though HPV11 E7 has a mostly nuclear phenotype, there is a consistent, low level of protein maintained in the cytoplasm, ostensibly due to the protein's interactions with cytoplasmic targets. However, the

equilibrium distribution of HPV11 E7 is decidedly in favor of nuclear import. Interestingly, this is not the case for the high risk HPV16 E7. The HPV16 cE7 displays a mostly cytoplasmic phenotype even though this region contains both a cNLS and a NES, suggesting that either the cNLS is weaker than that of HPV11 E7 or the NES is stronger than that of HPV11 E7 (Knapp, et al., 2009). The full length HPV16 E7 protein, though, does display a mostly nuclear phenotype like HPV11 E7 (Knapp, et al., 2009). Continued investigation of the differences between the nucleocytoplasmic transport of high risk HPV16 E7 and low risk HPV11 E7 will be informative regarding intrinsic cellular mechanisms for nucleocytoplasmic transport. Moreover, additional insights into the movement of the E7 oncoprotein within infected cells will be crucial for our understanding of HPV's prodigious ability to infect and transform mammalian cells and contribute to carcinogenesis.

Figures

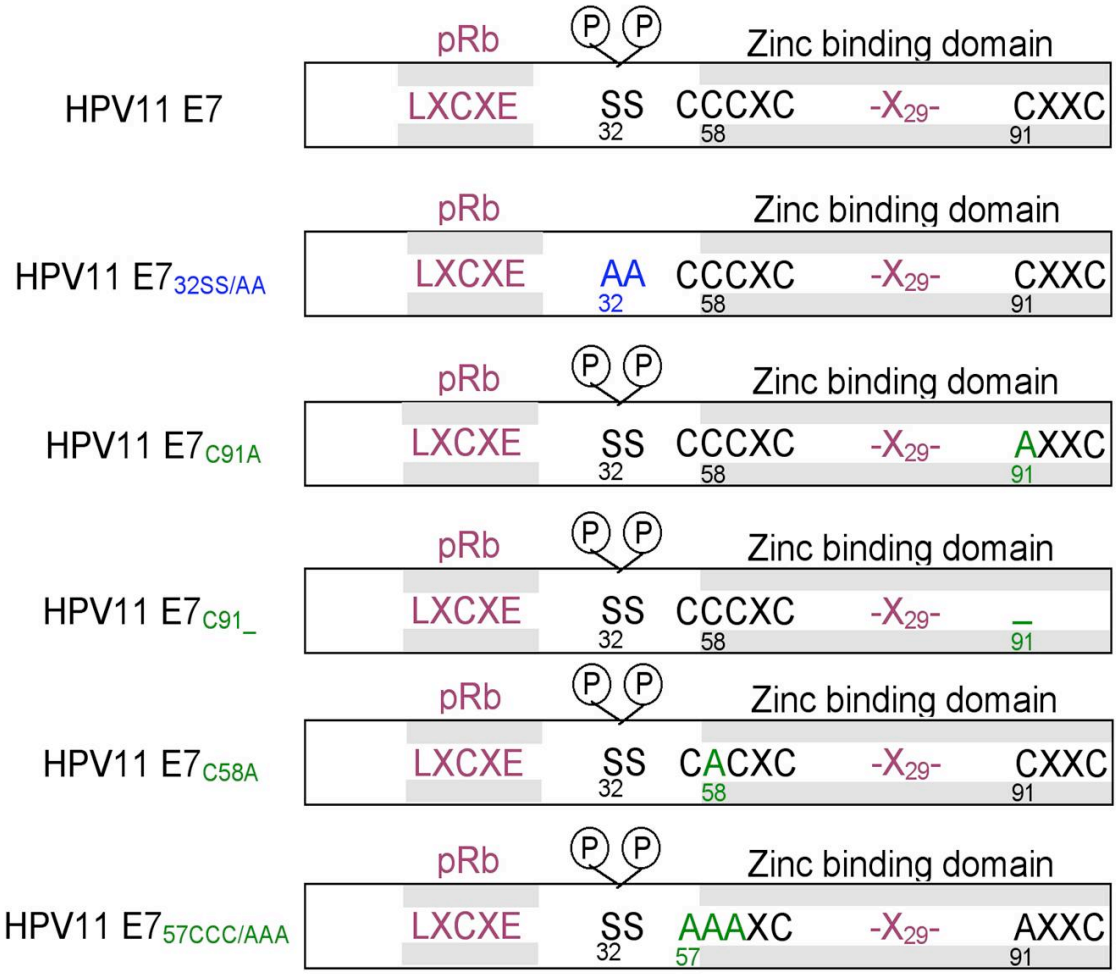

Figure 3A. Schematic representation of HPV11 E7 indicating the zinc-binding domain, the CKII phosphorylation sites, and the different mutations performed. Blue: CKII phosphorylation deficient mutation; Green: zinc-binding domain mutations.

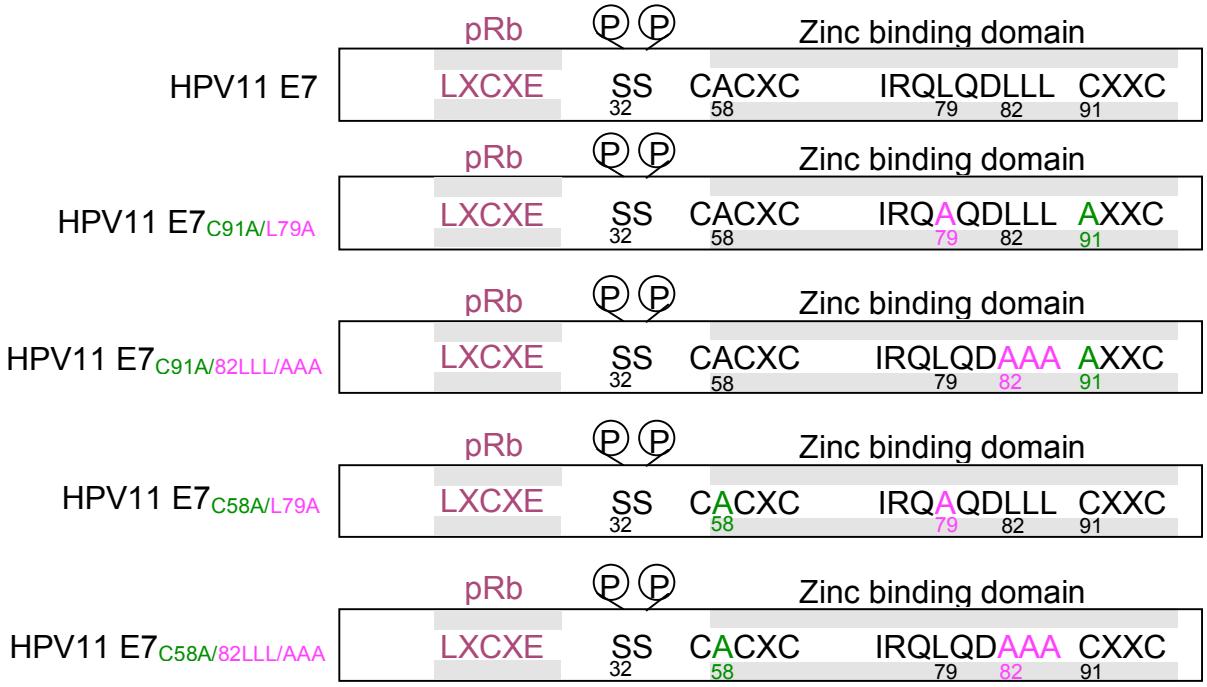

Figure 3B. Schematic representation of HPV11 E7 indicating the zinc-binding domain, the CKII phosphorylation sites, the proposed cNES, and the different mutations performed. Green: zinc-binding domain mutations; pink: cNES mutations.

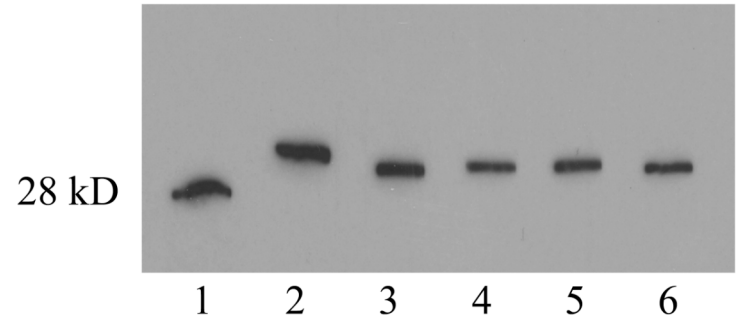

Figure 4A. Immunoblot analysis of EGFP-11cE7 and mutants used in transfection experiments. Lane 1: EGFP; Lane 2: EGFP-11cE7; Lane 3: EGFP-11cE7$_{C91A}$; Lane 4: EGFP-11cE7$_{C91_}$; Lane 5: EGFP-11cE7$_{C58A}$; Lane 6: EGFP-11cE7$_{57CCC/AAA}$

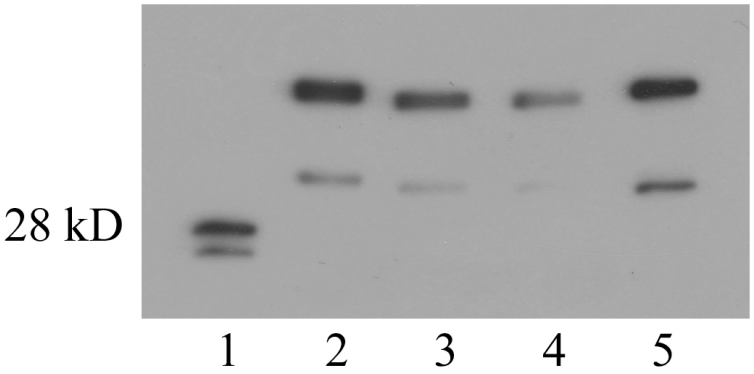

Figure 4B. Immunoblot analysis of EGFP-11E7 and mutants used in transfection experiments**.** Lane 1: EGFP; Lane 2: EGFP-11E7; Lane 3: EGFP-11E7$_{32SS/AA}$; Lane 4: EGFP-11E7$_{57CCC/AAA}$; Lane 5: EGFP-11E7$_{C91A}$

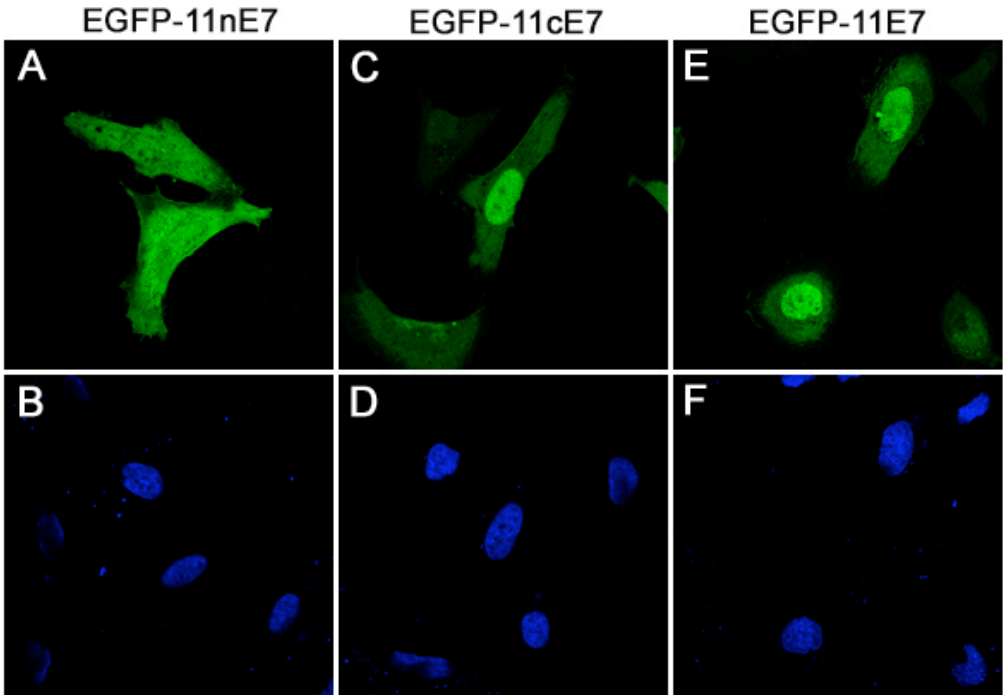

Figure 5A. EGFP-11E7 and EGFP-11E7$_{39-98}$ localize mostly to the nuclei of HeLa cells. HeLa cells were transfected with EGFP-11E7, EGFP-11nE7 and EGFP-11cE7 fusion plasmids as indicated in the figure and examined by fluorescence microscopy at 24 h post transfection. Panels A, C and E show the fluorescence of the EGFP and Panels B, D and F the DAPI staining of the nuclei.

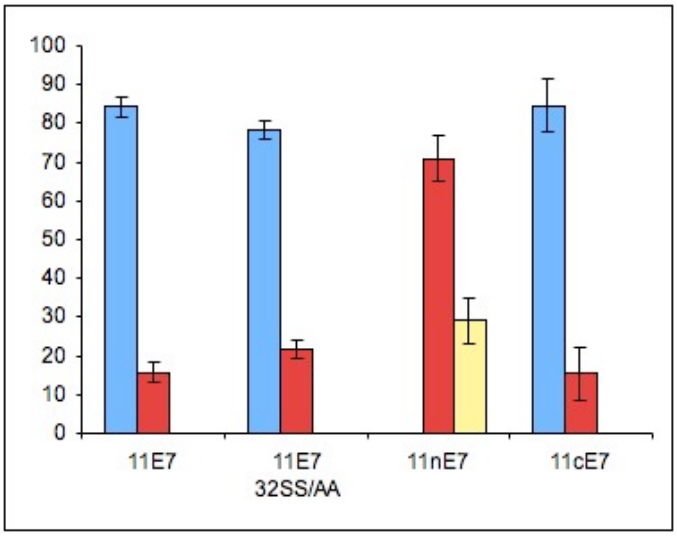

Figure 5B. Quantitative analysis of the localization of EGFP fusions with HPV11 E7 full length and its N and C domains. The data from experiments using EGFP-11E7, EGFP-$11E7_{32SS/AA}$, EGFP-11nE7, and EGFP-11cE7 plasmids have been used for quantitative analysis and the graphic representation of average with standard deviation. Mostly nuclear, blue bars; pancellular, red bars; cytoplasmic, yellow bars.

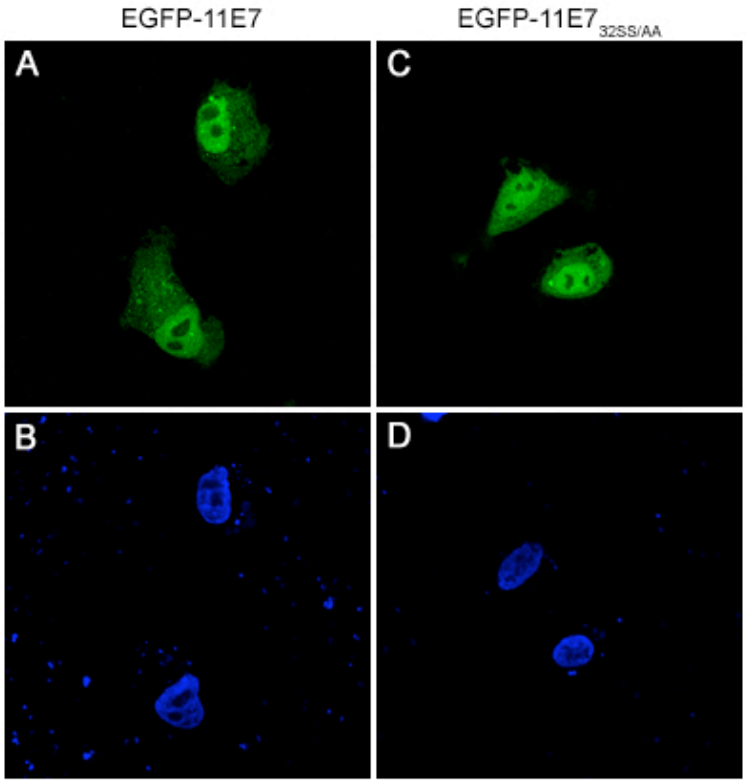

Figure 6. An HPV11 E7 variant deficient in CKII phosphorylation is mostly nuclear like the HPV11 E7 wild type. HeLa cells were transfected with either EGFP-11E7 wild type or EGFP-11E7$_{SS/AA}$ mutant and examined by fluorescence microscopy at 24 h post transfection. Panels A and C represent the fluorescence of the EGFP and panels B and D the DAPI staining of the nuclei.

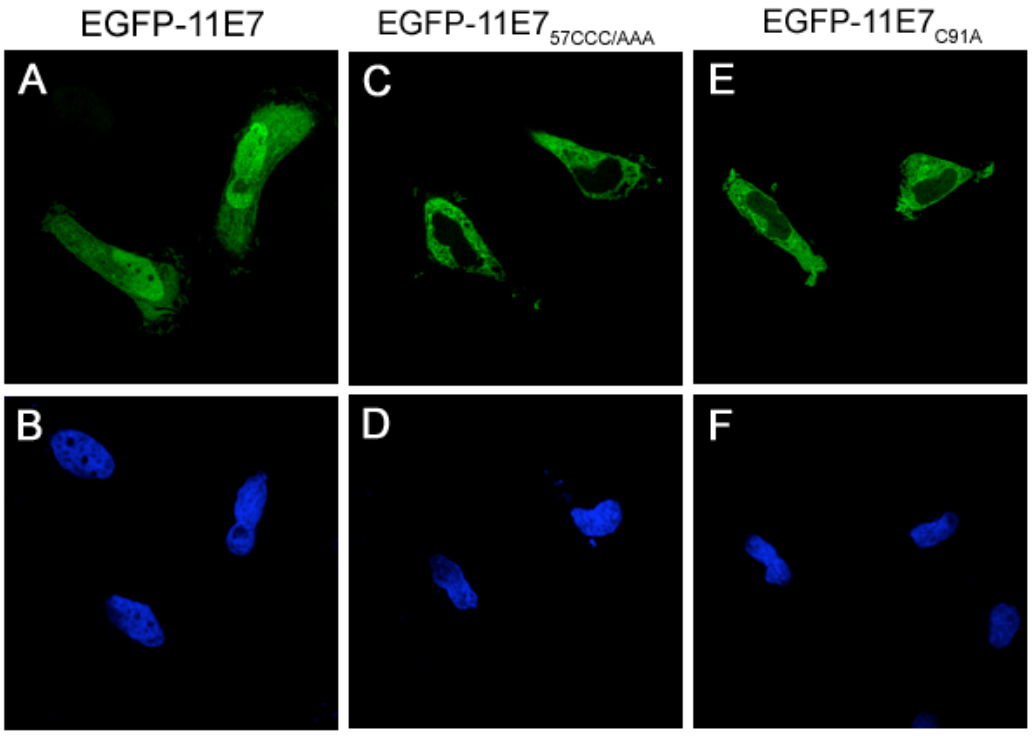

Figure 7A. The C91A and 57CCC/AAA mutations led to cytoplasmic localization of HPV11 E7 full length. HeLa cells were transfected with EGFP-11E7 (panels A and B), EGFP-11E7$_{57CCC/AAA}$ (panels C and D), and EGFP-11E7$_{C91A}$ (panels E and F) plasmids and examined by fluorescence microscopy at 24 h post transfection. Panels A, C, and E represent the fluorescence of the EGFP and panels B, D, and F the DAPI staining of the nuclei. Note the mostly nuclear localization of EGFP-11E7 wild type (panel A) and the cytoplasmic localization of EGFP-11E7$_{57CCC/AAA}$ (panel C) and EGFP-11E7$_{C91A}$ (panel E).

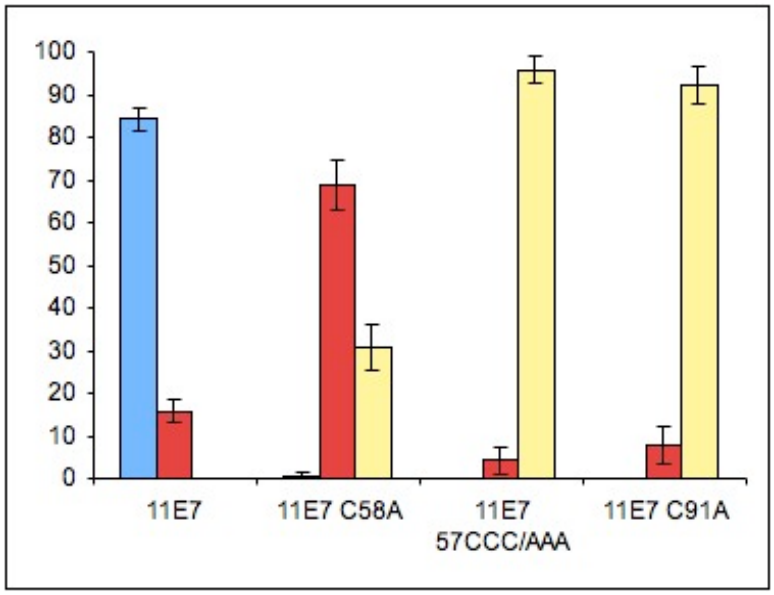

Figure 7B. Quantitative analysis of the intracellular localization of C58A, $_{57}$CCC/AAA, and C91A mutants in comparison with the wild type EGFP-11E7. The data from experiments using EGFP-11E7, EGFP-11E7$_{C58A}$, EGFP-11E7$_{57CCC/AAA}$, and EGFP-11E7$_{C91A}$ plasmids have been used for quantitative analysis and the graphic representation. Mostly nuclear, blue bars; pancellular, red bars; cytoplasmic, yellow bars.

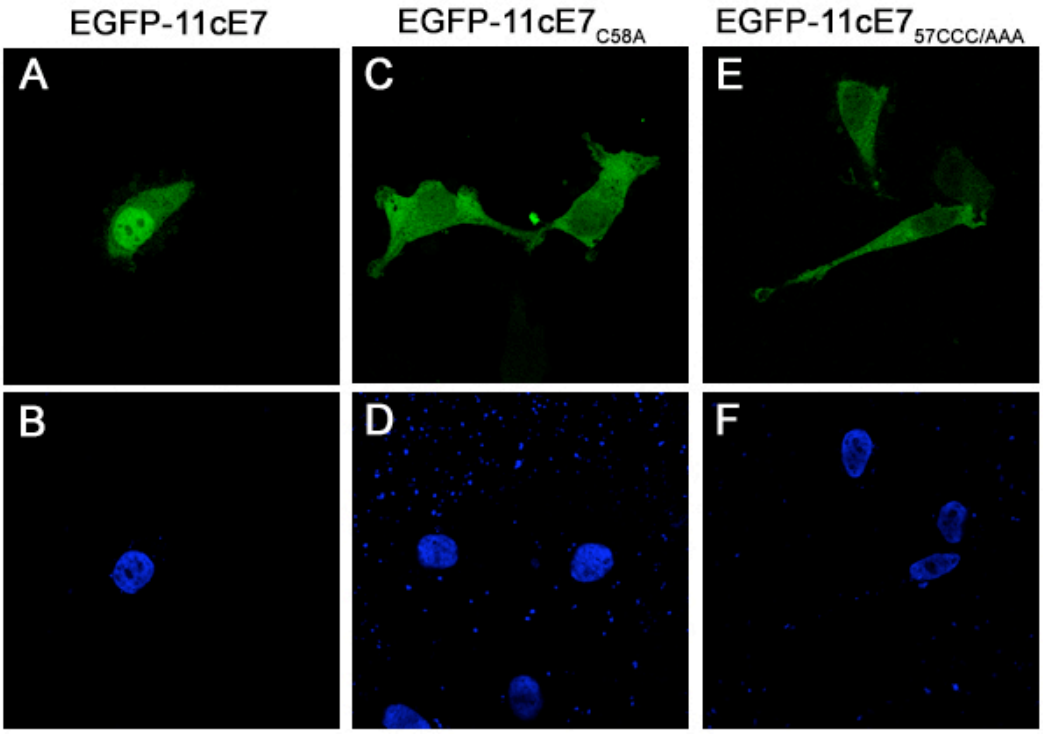

Figure 8A. The effect of C58A and 57CCC/AAA mutations on the localization of EGFP-11cE7. HeLa cells were transfected with either EGFP-11cE7 wild type (panels A and B), EGFP-11cE7$_{C58A}$ (panels C and D), and EGFP-11cE7$_{57CCC/AAA}$ (panels E and F) plasmids and examined by fluorescence microscopy at 24 h post transfection. Panels A, C, and E represent the fluorescence of the EGFP and panels B, D, and F the DAPI staining of the nuclei.

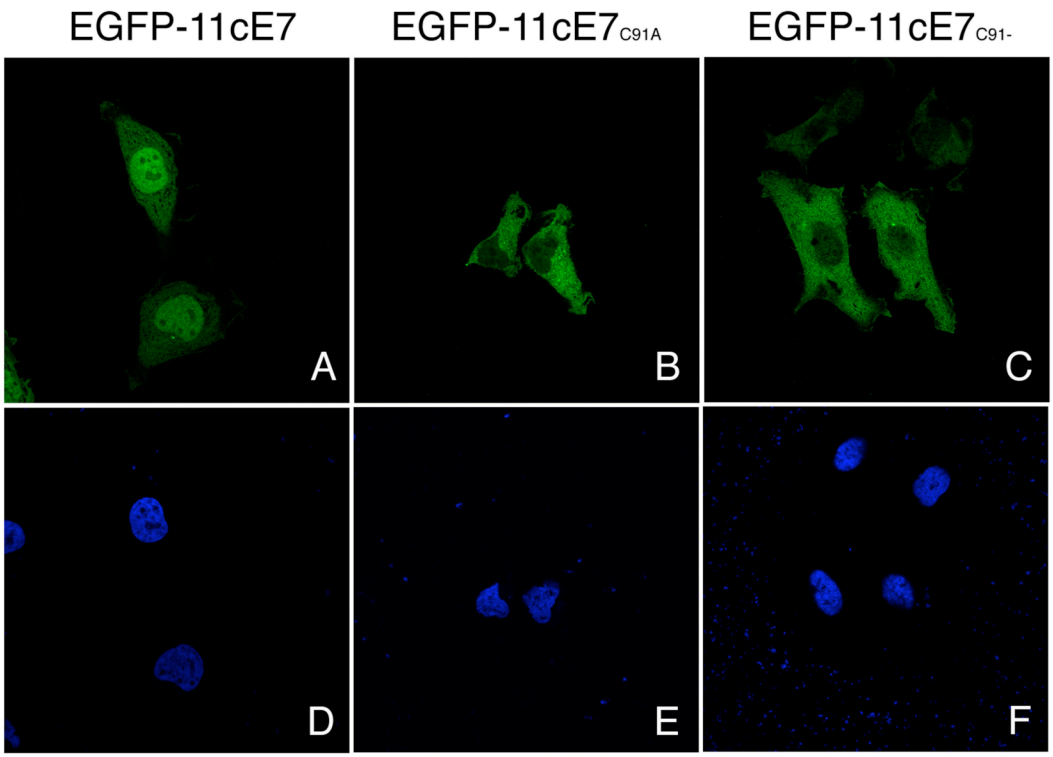

Figure 8B. The EGFP-11cE7$_{C91A}$ and EGFP-11cE7$_{C91_}$ mutants are localized mostly in the cytoplasm, in contrast with the mostly nuclear localization of the EGFP-11cE7 wild type. HeLa cells were transfected with either EGFP-11cE7 wild type (panels A and D), EGFP-11cE7$_{C91A}$ (panels B and E), or EGFP-11cE7$_{C91_}$ (panels C and F) plasmids and examined by fluorescence microscopy at 24 h post transfection. Panels A, B, and C represent the fluorescence of the EGFP and panels D, E, and F the DAPI staining of the nuclei.

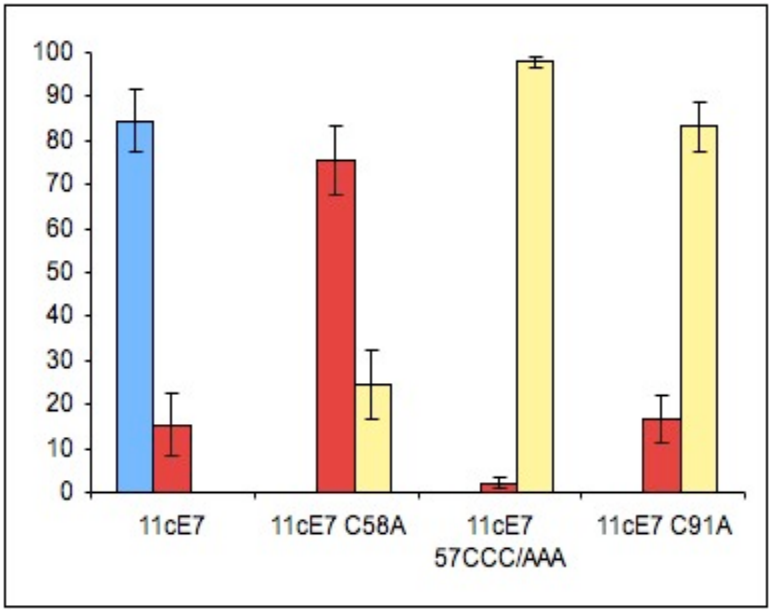

Figure 8C. Quantitative analysis of the intracellular localization of C58A, $_{57}$CCC/AAA, and C91A mutants in comparison with the wild type EGFP-11cE7. The data from experiments using EGFP-11cE7, EGFP-11cE7$_{C58A}$, EGFP-11cE7$_{57CCC/AAA}$, and EGFP-11cE7$_{C91A}$ plasmids have been used for quantitative analysis and the graphic representation. Mostly nuclear, blue bars; pancellular, red bars; cytoplasmic, yellow bars.

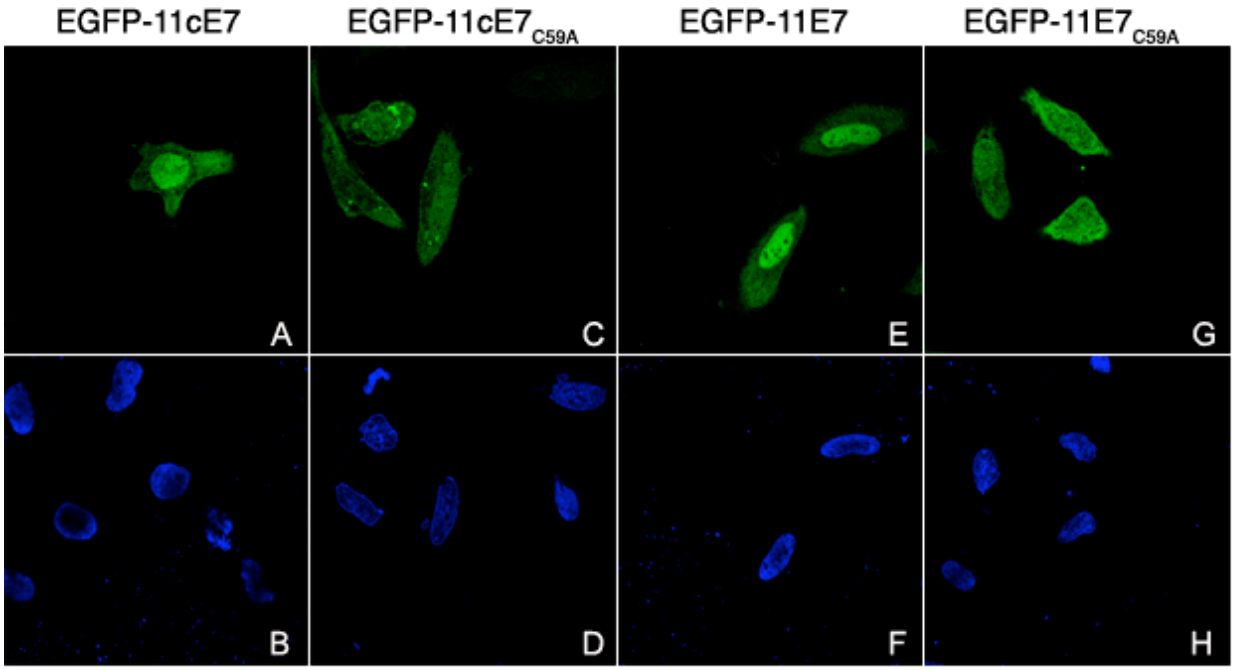

Figure 9A. The effect of C59A mutation on the localization of EGFP-c11E7 and EGFP-11E7. HeLa cells were transfected with EGFP-11cE7 (panels A and B), EGFP-11cE7$_{C59A}$ (panels C and D), EGFP-11E7 (panels E and F) and EGFP-11E7$_{C59A}$ (panels G and H) plasmids and examined by fluorescence microscopy at 24 h post transfection. Panels A, C, E, and G represent the fluorescence of the EGFP and panels B, D, F, and H the DAPI staining of the nuclei. Note the mostly nuclear localization of EGFP-11cE7 and EGFP-11E7 wild type (panels A and E) and pancellular localization of the C59A mutants (panels C and G). [Data thanks to Zeynep Onder]

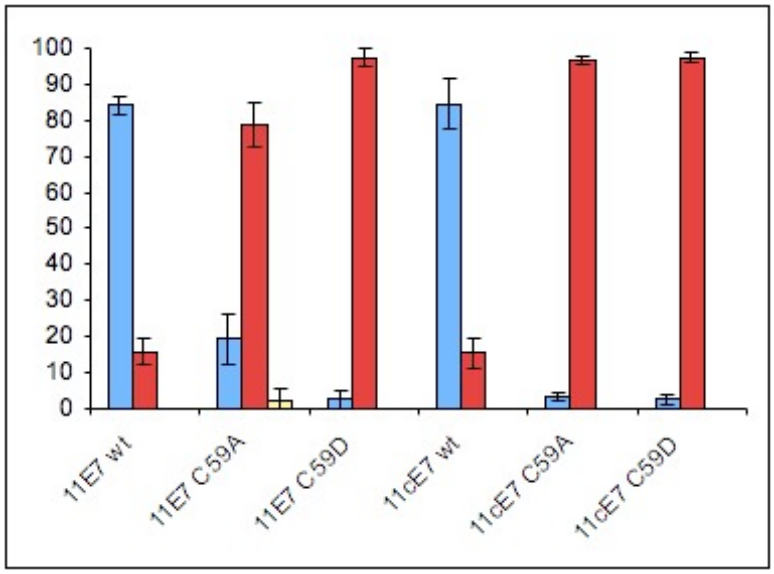

Figure 9B. Quantitative analysis of the intracellular localization of C59A and C59D mutants in comparison with the wild type EGFP-11E7 and EGFP-11cE7. The data from experiments using EGFP-11E7, EGFP-11cE7$_{C59A}$, EGFP-11E7$_{59D}$, EGFP-11cE7, EGFP-11cE7$_{C59A}$, EGFP-11cE7$_{C59D}$ plasmids have been used for quantitative analysis and the graphic representation. Mostly nuclear, blue bars; pancellular, red bars; cytoplasmic, yellow bars. [Data thanks to Zeynep Onder]

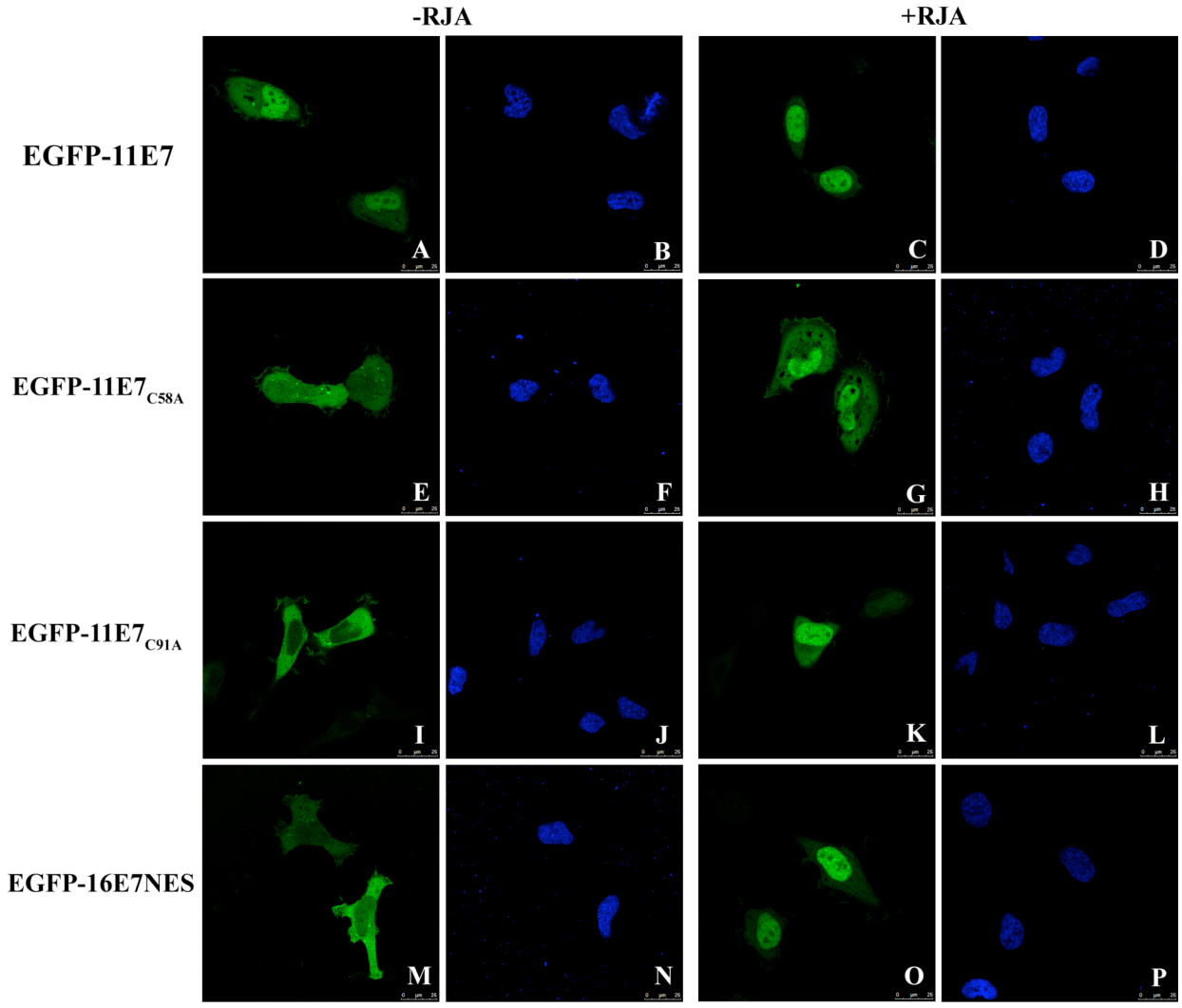

Figure 10A. The RJA nuclear export inhibitor partially restores the nuclear localization of EGFP-11E7 C58A and C91A mutants. HeLa cells were transfected with either EGFP-11E7 wild type (panels A-D), EGFP-11E7$_{C58A}$ (panels E-H), EGFP-11E7$_{C91A}$ (panels I-L), and EGFP-16E7NES (panels M-P) plasmids in the absence of any drug or in the presence of RJA and examined by fluorescence microscopy at 24 h post transfection. Panels A, C, E, G, I, K, M, and O represent the fluorescence of the EGFP and panels B, D, F, H, J, L, N, and P the DAPI staining of the nuclei.

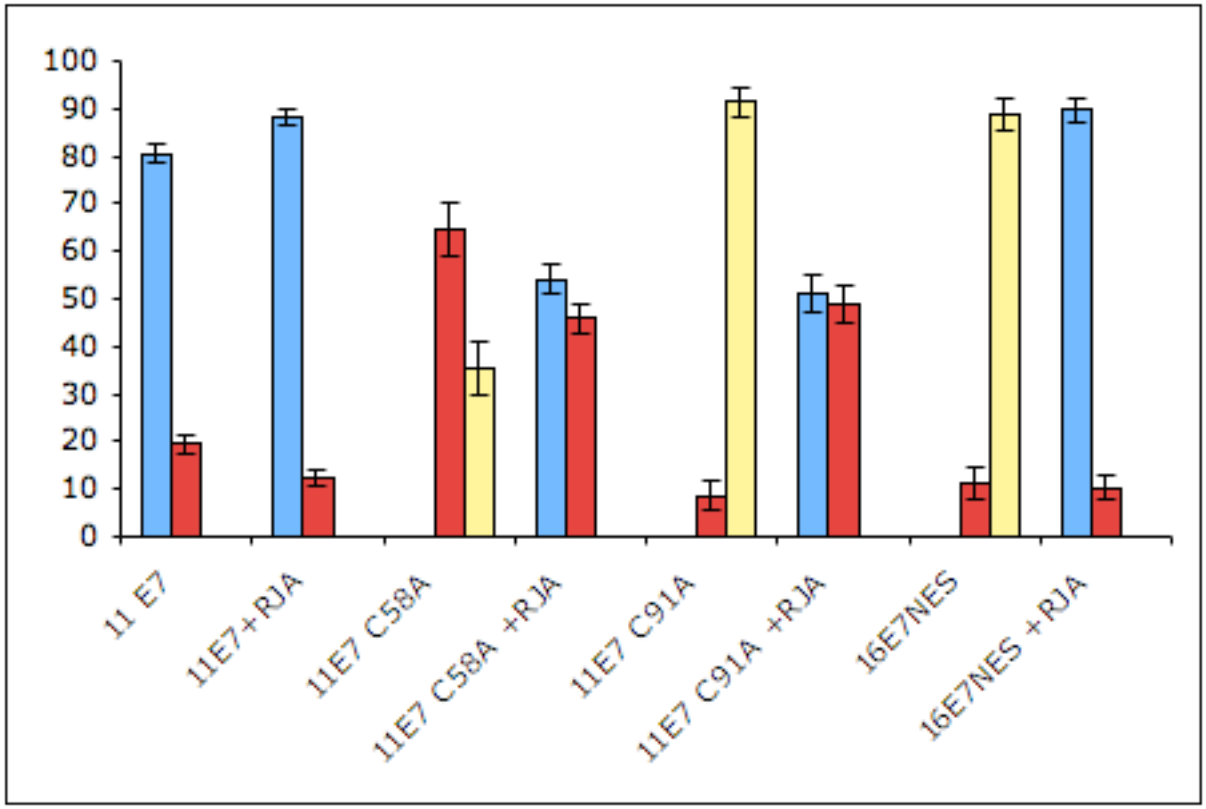

Figure 10B. Quantitative analysis of the effect of RJA on the localization of the EGFP-11E7 C58A and C91A mutants. The data from experiments using EGFP-11E7, EGFP-11E7$_{C58A}$, EGFP-11E7$_{C91A}$, and EGFP-16E7NES plasmids, with or without RJA treatment, have been used for quantitative analysis and the graphic representation. Mostly nuclear, blue bars; pancellular, red bars; cytoplasmic, yellow bars.

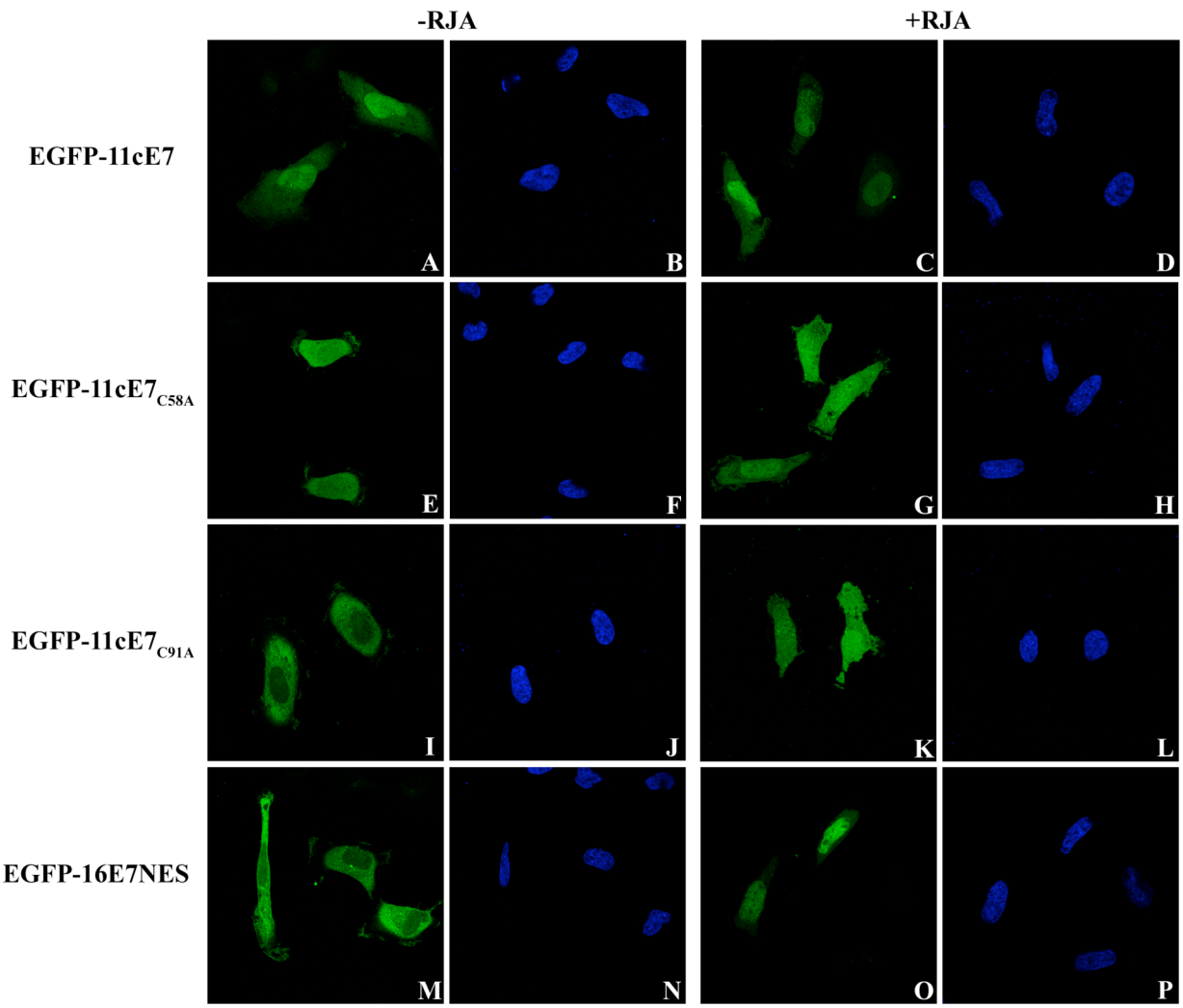

Figure 11A. The RJA nuclear export inhibitor partially restores the nuclear localization of EGFP-11cE7 C58A and C91A mutants. HeLa cells were transfected with either EGFP-11cE7 wild type (panels A-D), EGFP-11cE7$_{C58A}$ (panels E-H), EGFP-11cE7$_{C91A}$ (panels I-L), and EGFP-16E7NES (panels M-P) plasmids in the absence of any drug or in the presence of RJA and examined by fluorescence microscopy at 24 h post transfection. Panels A, C, E, G, I, K, M, and O represent the fluorescence of the EGFP and panels B, D, F, H, J, L, N, and P the DAPI staining of the nuclei.

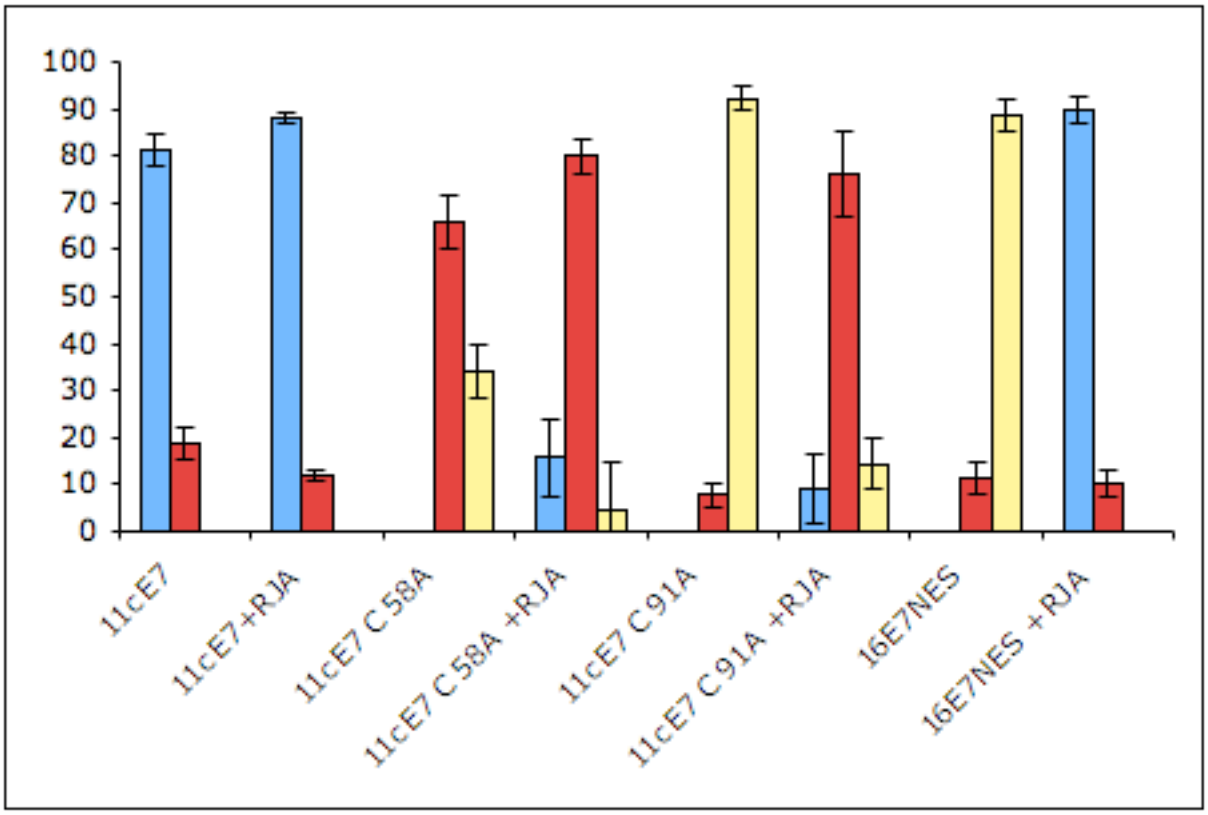

Figure 11B. Quantitative analysis of the effect of RJA on the localization of EGFP-11cE7 C58A and C91A mutants. The data from experiments using EGFP-11cE7, EGFP-11cE7$_{C58A}$, EGFP-11cE7$_{C91A}$, and EGFP-16E7NES plasmids, with or without RJA treatment, have been used for quantitative analysis and the graphic representation. Mostly nuclear, blue bars; pancellular, red bars; cytoplasmic, yellow bars.

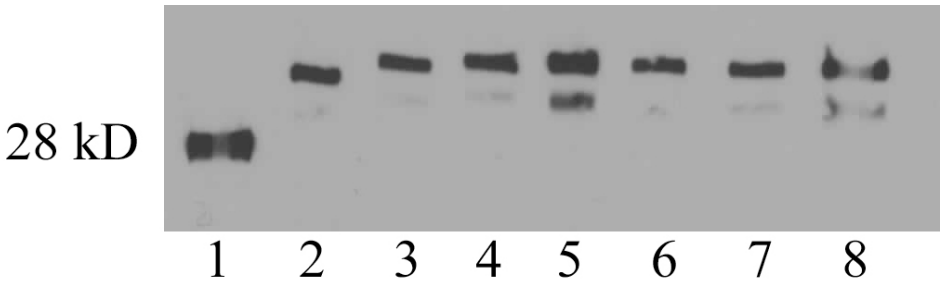

Figure 12. Immunoblot analysis of EGFP-11E7 and mutants used in transfection experiments. Lane 1: EGFP; Lane 2: EGFP-11E7; Lane 3: EGFP-11E7$_{C58A}$; Lane 4: EGFP-11E7$_{C58A/L79A}$; Lane 5: EGFP-11E7$_{C58A/82LLL/AAA}$; Lane 6: EGFP-11E7$_{C91A}$; Lane 7: EGFP-11E7$_{C91A/L79A}$; Lane 8: EGFP-11E7$_{C91A/82LLL/AAA}$

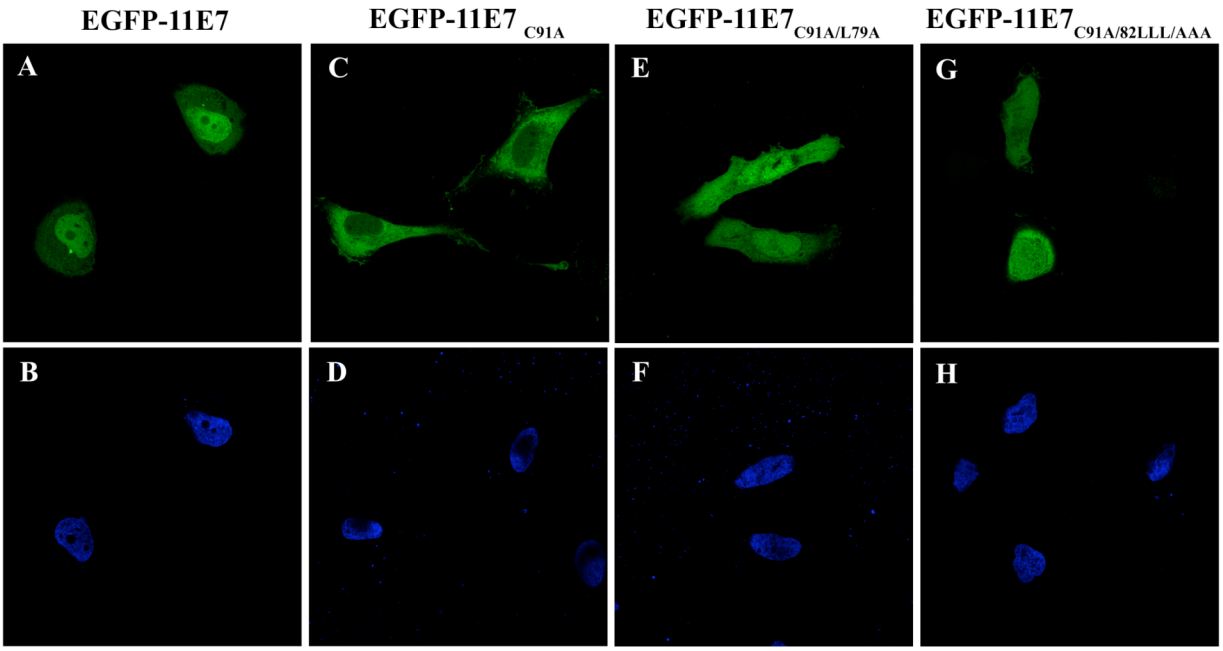

Figure 13A. Mutations of critical leucine residues in a potential cNES change the localization of the EGFP-11E7 C91A mutant. HeLa cells were transfected with either EGFP-11E7 wild type (panels A and B), EGFP-11E7$_{C91A}$ (panels C and D), EGFP-11E7$_{C91A/L79A}$ (panels E and F), and EGFP-11E7$_{C91A/82LLL/AAA}$ (panels G and H) plasmids and examined by fluorescence microscopy at 24 h post transfection. Panels A, C, E, and G represent the fluorescence of the EGFP and panels B, D, F, and H the DAPI staining of the nuclei.

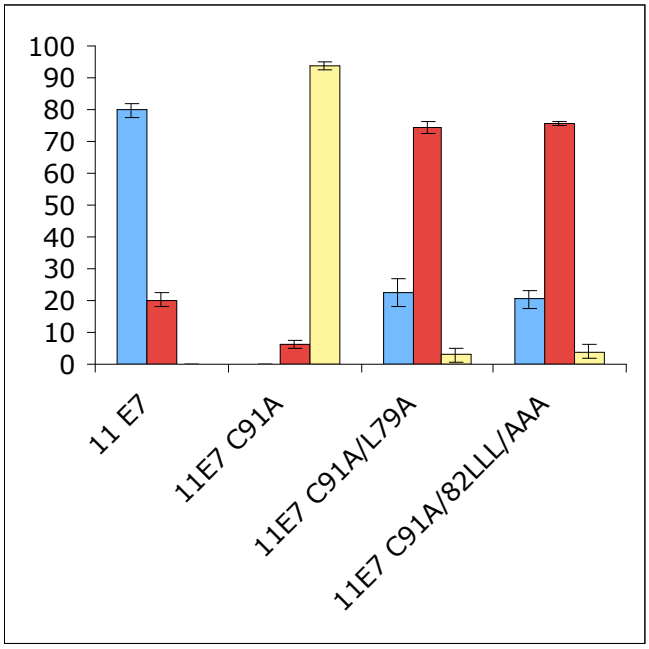

Figure 13B. Quantitative analysis of the effect of mutations of critical leucine residues in a potential cNES on the localization of the EGFP-11E7 C91A mutant. The data from experiments using EGFP-11E7, EGFP-11E7$_{C91A}$, EGFP-11E7$_{C91A/L79A}$, and EGFP-11E7$_{C91A/82LLL/AAA}$ plasmids have been used for quantitative analysis and the graphic representation. Mostly nuclear, blue bars; pancellular, red bars; cytoplasmic, yellow bars.

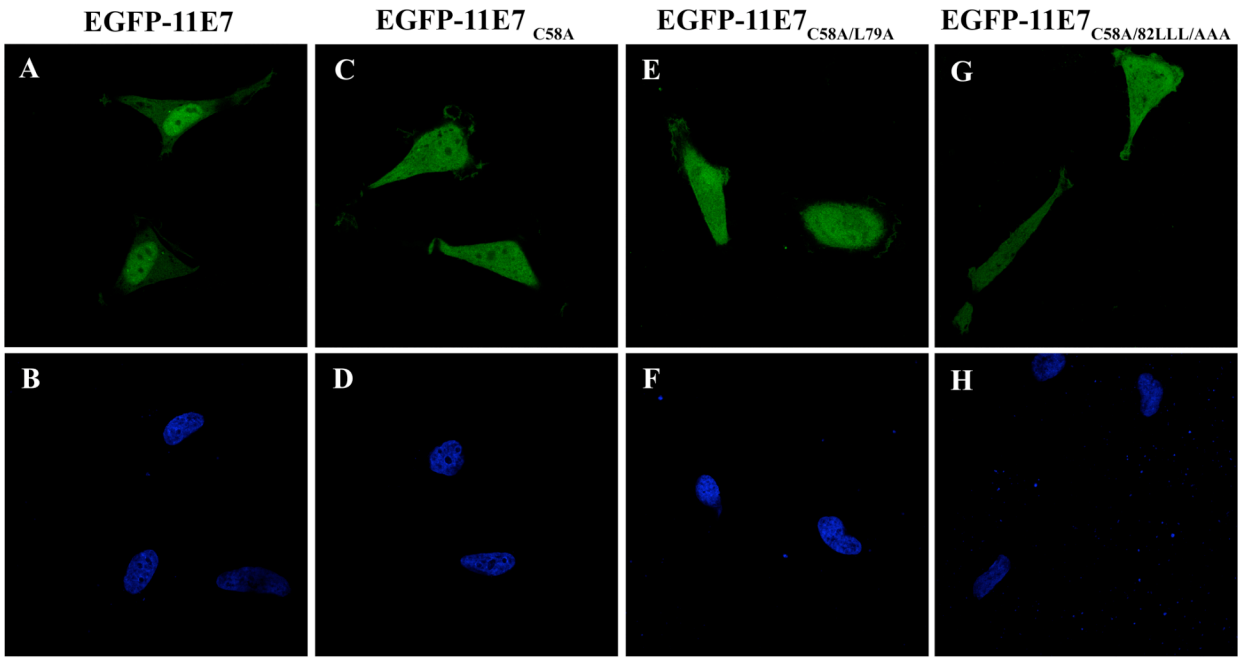

Figure 14A. Mutations of critical leucine residues in a potential cNES change the localization of the EGFP-11E7 C58A mutant. HeLa cells were transfected with either EGFP-11E7 wild type (panels A and B), EGFP-11E7$_{C58A}$ (panels C and D), EGFP-11E7$_{C58A/L79A}$ (panels E and F), and EGFP-11E7$_{C58A/82LLL/AAA}$ (panels G and H) plasmids and examined by fluorescence microscopy at 24 h post transfection. Panels A, C, E, and G represent the fluorescence of the EGFP and panels B, D, F, and H the DAPI staining of the nuclei.

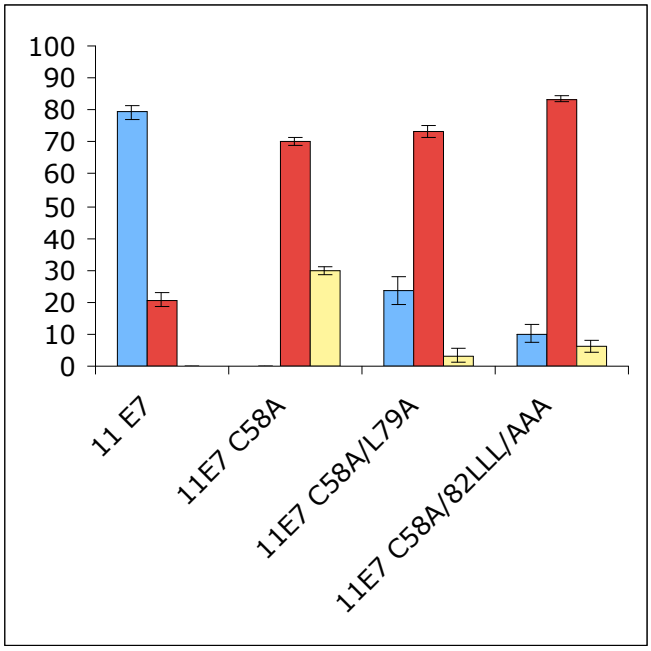

Figure 14B. Quantitative analysis of the effect of mutations of critical leucine residues in a potential cNES on the localization of the EGFP-11E7 C58A mutant. The data from experiments using EGFP-11E7, EGFP-11E7$_{C58A}$, EGFP-11E7$_{C58A/L79A}$, and EGFP-11E7$_{C58A/82LLL/AAA}$ plasmids have been used for quantitative analysis and the graphic representation. Mostly nuclear, blue bars; pancellular, red bars; cytoplasmic, yellow bars.

References

Alber, F., Dokudovskaya, S., Veenhoff, L., Zhang, W., Kipper, J., Devos, D., Suprapto, A., Karni-Schmidt, O., Williams, R., Chait, B., Sali, A., and Rout, M. (2007). The molecular architecture of the nuclear pore complex. *Nature*; 750:695-701

Angeline, M., Merle, E., and Moroianu, J. (2003). The E7 oncoprotein of high-risk human papillomavirus type 16 enters the nucleus via a nonclassical ran-dependent pathway. *Virology; 317*(1):13-23.

Clemens, K. E., Brent, R., Gyuris, J., and Munger, K. (1995). Dimerization of the human papillomavirus E7 oncoprotein *in vivo*. *Virology; 214*(1):289-293.

Doorbar, J. (2006). Molecular biology of human papillomavirus infection and cervical cancer. *Clin Sci* (Lond); 110:525-41.

Dunne, E. F., Unger, E. R., Sternberg, M., McQuillan, G., Swan, D. C., Patel, S. S., and Markowitz, L. E. (2007). Prevalence of HPV infection among females in the United States. *JAMA; 297*(8):813-819.

Fahrenkrog, B. and Aebi, U. (2003). The nuclear pore complex: nucleocytoplasmic transport and beyond. *Nature Reviews Molecular Cell Biology;* 4:757-766.

Fornerod, M., Ohno, M., Yoshida, M., and Mattaj, I. W. (1997). CRM1 is an export receptor for leucine-rich nuclear export signals. *Cell;* 90:1051-60.

Heck, D., Yee, C., Howley, P., and Munger, K. (1992). Efficiency of binding the retinoblastoma protein correlates with the transforming capacity of the E7 oncoproteins of the human papillomaviruses. *Proc Natl Acad Sci USA*; *89*(10):4442-6.

Knapp, A. A., McManus, P. M., Bockstall, K., and Moroianu, J. (2009). Identification of the nuclear localization and export signals of high risk HPV16 E7 oncoprotein. *Virology; 383*(1):60-68.

Longworth, M. S. and Laimins, L. A. (2004). Pathogenesis of human papillomaviruses in differentiating epithelia. *Microbiol. Mol. Biol. Rev.; 68*(2):362-372.

Malim, M. H., McCarn, D. F., Tiley, L. S., and Cullen, B. R. (1991). Mutational definition of the human immunodeficiency virus type 1 Rev activation domain. *J. Virol.;* 65:4248–4254.

Moody, C. and Laimins, L. (2010). Human papillomavirus oncoproteins: pathways to transformation. *Nature Reviews Cancer;* 10:550-560.

Moroianu, J. (1999). Nuclear import and export pathways. *Journal of Cellular Biochemistry; 75*(32):76-83.

McLaughlin-Drubin, M. and Munger, K. (2008). The human papillomavirus E7 oncoprotein. *Virology;* 384:335–344.

Ohlenschlager, O., Seiboth, T., Zengerling, H., Briese, L., Marchanka, A., Ramachandran, R., Baum, M., Korbas, M., Meyer-Klaucke, W., Durst, M., and Gorlach, M. (2006). Solution structure of the partially folded high-risk human papillomavirus 45 oncoprotein E7. *Oncogene; 25*(44):953–5959.

Parkin, D. M., Bray, F., Ferlay, J., and Pisani, P. (2002). Global cancer statistics. *CA Cancer J Clin*; *55*(2):74-108.

Pemberton, L. F. and Paschal, B. M. (2005). Mechanisms of receptor-mediated nuclear import and nuclear export. *Traffic;* 6:187-98.

Pfister, H. (2003). Human Papillomavirus and Skin Cancer. *Journal of the National Cancer Institute Monograms;* 31:52–56.

Piccioli, Z., McKee, C. H., Leszczynski, A., Onder, Z., Hannah, E. C., Mamoor, S., Crosby, L., Moroianu, J. (2010). The nuclear localization of low risk HPV11 E7 protein mediated by its zinc binding domain is independent of nuclear import receptors. *Virology; 407*(1):100-109.

Ribbeck, K. and Gorlich, D. (2002). The permeability barrier of nuclear pore complexes appears to operate via hydrophobic exclusion. *EMBO J.;* 21:2664–2671.

Sorokin, A. V., Kim, E. R., and Ovchinnikov, L. P. (2007). Nucleocytoplasmic transport of proteins. *Biochemistry* (Mosc); 72:1439-57.

zur Hausen, H. (2000). Papillomaviruses Causing Cancer: Evasion From Host-Cell Control in Early Events in Carcinogenesis. *Journal of the National Cancer Institute; 92*(9):690-698.